Approved for public release; distribution is unlimited.

Solid Fuel Ramjet
Infrared Signature

by

Russell P. Luehrsen
Lieutenant, United States Navy
B.S., United States Naval Academy

Submitted in partial fulfillment
of the requirements for the degree of

MASTER OF SCIENCE IN AEROSPACE ENGINEERING

from the

NAVAL POSTGRADUATE SCHOOL
December 1990

Department of Aeronautics and Astronautics

SECURITY CLASSIFICATION OF THIS PAGE

REPORT DOCUMENTATION PAGE

Form Approved
OMB No. 0704-0188

1a REPORT SECURITY CLASSIFICATION Unclassified	1b RESTRICTIVE MARKINGS Approved for public release; distribution is unlimited.
2a SECURITY CLASSIFICATION AUTHORITY	3 DISTRIBUTION/AVAILABILITY OF REPORT
2b DECLASSIFICATION/DOWNGRADING SCHEDULE	
4 PERFORMING ORGANIZATION REPORT NUMBER(S)	5 MONITORING ORGANIZATION REPORT NUMBER(S)
6a NAME OF PERFORMING ORGANIZATION Naval Postgraduate School 6b OFFICE SYMBOL (If applicable) AA	7a NAME OF MONITORING ORGANIZATION Naval Postgraduate School
6c ADDRESS (City, State, and ZIP Code) Monterey, CA 93943-5000	7b ADDRESS (City, State, and ZIP Code) Monterey, CA 93943-5000
8a NAME OF FUNDING/SPONSORING ORGANIZATION Naval Weapons Center 8b OFFICE SYMBOL (If applicable)	9 PROCUREMENT INSTRUMENT IDENTIFICATION NUMBER
8c ADDRESS (City, State, and ZIP Code) China Lake, CA 93555	10 SOURCE OF FUNDING NUMBERS PROGRAM ELEMENT NO PROJECT NO N60530 91WR30042 TASK NO WORK UNIT ACCESSION NO

11 TITLE (Include Security Classification)

Solid Fuel Ramjet Infrared Signature

12 PERSONAL AUTHOR(S)

Luehrsen, Russell P.

13a TYPE OF REPORT	13b TIME COVERED	14 DATE OF REPORT (Year, Month, Day)	15 PAGE COUNT
Master's Thesis	FROM _____ TO _____	1991 December	76

16 SUPPLEMENTARY NOTATION The views expressed in this thesis are those of the author and do not reflect the official policy or position of theDeparment of Defense or the US Government.

17 COSATI CODES			18 SUBJECT TERMS (Continue on reverse if necessary and identify by block number)
FIELD	GROUP	SUB-GROUP	Ramjet; Solid Fuel; Infrared Signature

19 ABSTRACT (Continue on reverse if necessary and identify by block number)

The objective of the thesis was to determine the effects of equivalence ratio and fuel composition on the infrared signature of solid fueled ramjets (SFRJ). Solid fuel investigated were Plexiglas, HTPB, and HTPB with aluminum, silicon, boron carbide, and/or magnesium. They were tested at chamber pressures of 80-170 psia and with equivalence ratios between 0.3 and 1.4. With the plume emissivity set to 1.0, plume irradiance was found to increase approximately with the second power of the actual combustor stagnation temperature. In addition to providing needed plume signature data for the SFRJ, this information can be used to validate numerical predictions from the SPF (Standardized Plume Flowfield) and SIRRM (Standardized Infrared Radiation Model) computer codes, which are used to predict the plume infrared signature.

20 DISTRIBUTION/AVAILABILITY OF ABSTRACT	21 ABSTRACT SECURITY CLASSIFICATION
☒ UNCLASSIFIED/UNLIMITED ☐ SAME AS RPT ☐ DTIC USERS	Unclassified
22a NAME OF RESPONSIBLE INDIVIDUAL Prof. David W. Netzer	22b TELEPHONE (Include Area Code) (408) 646-2980 22c OFFICE SYMBOL AA/Nt

DD Form 1473, JUN 86 *Previous editions are obsolete.* SECURITY CLASSIFICATION OF THIS PAGE

S/N 0102-LF-014-6603

NAVAL POSTGRADUATE SCHOOL
Monterey , California

THESIS

SOLID FUEL RAMJET
INFRARED SIGNATURE

by

Russell P. Luehrsen

December, 1991

Thesis Advisor: David W. Netzer

ABSTRACT

The objective of the thesis was to determine the effects of equivalence ratio (ϕ) and fuel composition on the infrared signature of solid fueled ramjets (SFRJ). Solid fuels investigated were Plexiglas, HTPB, and HTPB with aluminum, silicon, boron carbide, and/or magnesium. They were tested at chamber pressures of 80-170 psia and with equivalence ratios between 0.3 and 1.4. With the plume emissivity set to 1.0, plume irradiance was found to increase approximately with the second power of the actual combustor stagnation temperature. In addition to providing needed plume signature data for the SFRJ, this information can be used to validate numerical predictions from the SPF (Standardized Plume Flowfield) and SIRRM (Standardized Infrared Radiation Model) computer codes, which are used to predict the plume infrared signature.

TABLE OF CONTENTS

LIST OF TABLES

LISTS OF FIGURES

LIST OF SYMBOLS

A	Throat area (in^2)
B	Spectral factor
C_D	Nozzle discharge coefficient
c	Speed of light (2.998×10^8 m/s)
D_{cam}	Object's distance from the camera
$d_{f\ ave}$	Post-firing average inner fuel diameter
$d_{i\ ave}$	Initial average internal fuel diameter
F	Internal thrust with a perfectly expanded nozzle
F_c	Shape factor
F_s	Static thrust
f	Fuel-air ratio ($\dot{m}_f/\dot{m}_a$)
f_{stoich}	Stoichiometric fuel air ratio
g_c	Unit conversion factor (32.174 lb_m ft/ lb_f sec^2)
g_o	Gravitational constant
h	Planck's constant (6.626×10^{-34} J s)
I	Thermal value
Isp	Specific impulse
Isp_s	Static specific impulse
K	Mass flow rate conversion
k	Boltzmann's constant (1.3807×10^{-23} J/K)
L_{probe}	Length from the nozzle exit to plume probes
L_{fuel}	Length of the fuel grain
M	Mach number
M_b	Black body radiant emittance (W/m^2)
$M_{\lambda b}$	Black body spectral radiant emittance (W/m^3)
MW	Molecular Weight
m	Mass

$\dot{m}$	Mass flow rate
$\dot{m}_a$	Air mass flow rate mixing with the plume
$\dot{m}_e$	Mass flow rate at the nozzle exit
$\dot{m}_f$	Mass flow rate of the fuel
$\dot{m}_g$	Total gas mass flow rate
$\dot{m}_h$	Heater hydrogen mass flow rate
$\dot{m}_o$	Air mass flow rate at the inlet
$\dot{m}_{ox}$	Heater oxygen mass flow rate
$\dot{m}_{total}$	Total mass flow rate
Δm	Change in mass
N_{cam}	Camera received photon intensity
N_o	Object transmitted photon intensity
N_λ	Photon intensity per wavelength
P	Static pressure (psia)
P_t	Stagnation press (psia)
R	Universal gas constant (ft lb_f/mole °R)
R_c	Response factor
$\dot{r}$	Fuel regression rate
SFC	Specific fuel consumption
T	Static temperature
$T_{cam\ ave}$	Average plume temperature by the IR camera
$T_{cam\ max}$	Maximum plume temperature by the IR camera
T_{plume}	Plume static temperature
$T_{t\ plume}$	Non-water-cooled plume stagnation temperature
$T_{tc\ plume}$	Water-cooled plume stagnation temperature
T_t	Stagnation temperature
u_e	Velocity at the nozzle exit
u_o	Velocity at the inlet
α	Absorption coefficient
ε	Emissivity
ε_o	Object emissivity

γ	Specific heat ratio
η	Combustion efficiency
ρ	Reflection coefficient
ρ_{fuel}	Fuel density
τ	Transmission coefficient
ϕ	Equivalence ratio, f/f_{stoich}
λ	Wavelength (m)
σ	Stefan-Boltzmann constant (5.67051×10^{-12} W/cm^2 K^4)

Subscript

b	Burn
p	Pre-ignition
th	Theoretical

I. INTRODUCTION

A. BACKGROUND

As the air-breathing missile's speed increases above Mach 2.5, the advantages of ramjet propulsion in specific fuel consumption (SFC) and specific impulse (Isp) make it the optimum propulsion choice (Figure 1). The solid fueled ramjet also offers a "low cost, self-throttling, simple design that is well suited for a high-g environment" [Ref. 1:p. 186]. Its major disadvantages include a "possible lower combustion efficiency, performance dependent upon altitude and speed, required aft mixing chamber, fuel exposed to booster pressures, and the need for the air inlets to be more forward than for liquid fueled ramjets or turbojets" [Ref. 1:p. 186]. To track and counter this high speed missile, all means available including, infrared, radar, and other electronic emissions must be considered. From an offensive standpoint, it is desirable to maintain the missiles signature as small as possible to prevent detection.

The two performance criteria mentioned earlier are obtained for ideal nozzle expansion by,

$$F = \dot{m}_e u_e - \dot{m}_o u_o = \dot{m}_o[(1+f)u_e - u_o]$$

$$SFC = \dot{m}_f / F$$

$$Isp = F/\dot{m}_f g_o$$

It is important to note that ramjet "performance depends upon both the fuel-air ratio and flight conditions" [Ref. 2:p. 185]. For performance evaluations between various engines, the flight condition variables should be excluded. As discussed in Reference 2, this can be done by using a "static thrust", $F_s = \dot{m}_o(1+f)u_e$, to calculate a static specific impulse, Isp_s. It can be shown that Isp_s is directly proportional to the heat

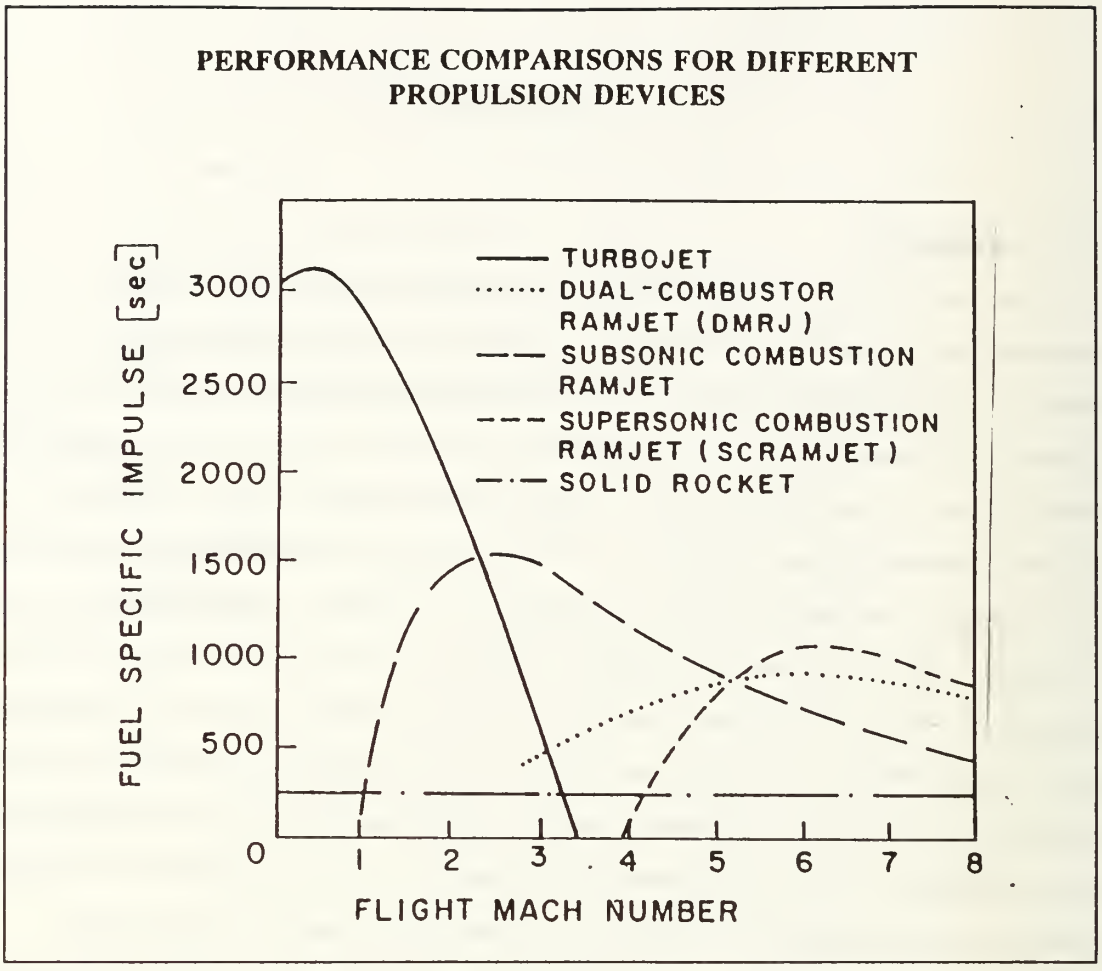

FIGURE 1: Performance Comparisons for Different Propulsion Devices. Adapted from [Ref. 3:p. 139-154]

released per unit mass of fuel. By adding certain metals (such as aluminum, boron, magnesium, silicon, and/or metal hydrides of these elements) to the fuel, the heat of combustion per unit mass and unit volume can be increased (Figure 2). Beryllium is very toxic and not recommended as a fuel additive. The heat of combustion is directly related to the heat added to the system. This will allow for a higher transfer of energy per unit mass of fuel to the ramjet gases, thus improving the Isp and decreasing the SFC. [Ref. 2:pp. 158-162] However, this additional heat will cause the temperature in the ramjet combustor and plume to increase, thus increasing the infrared signature. The

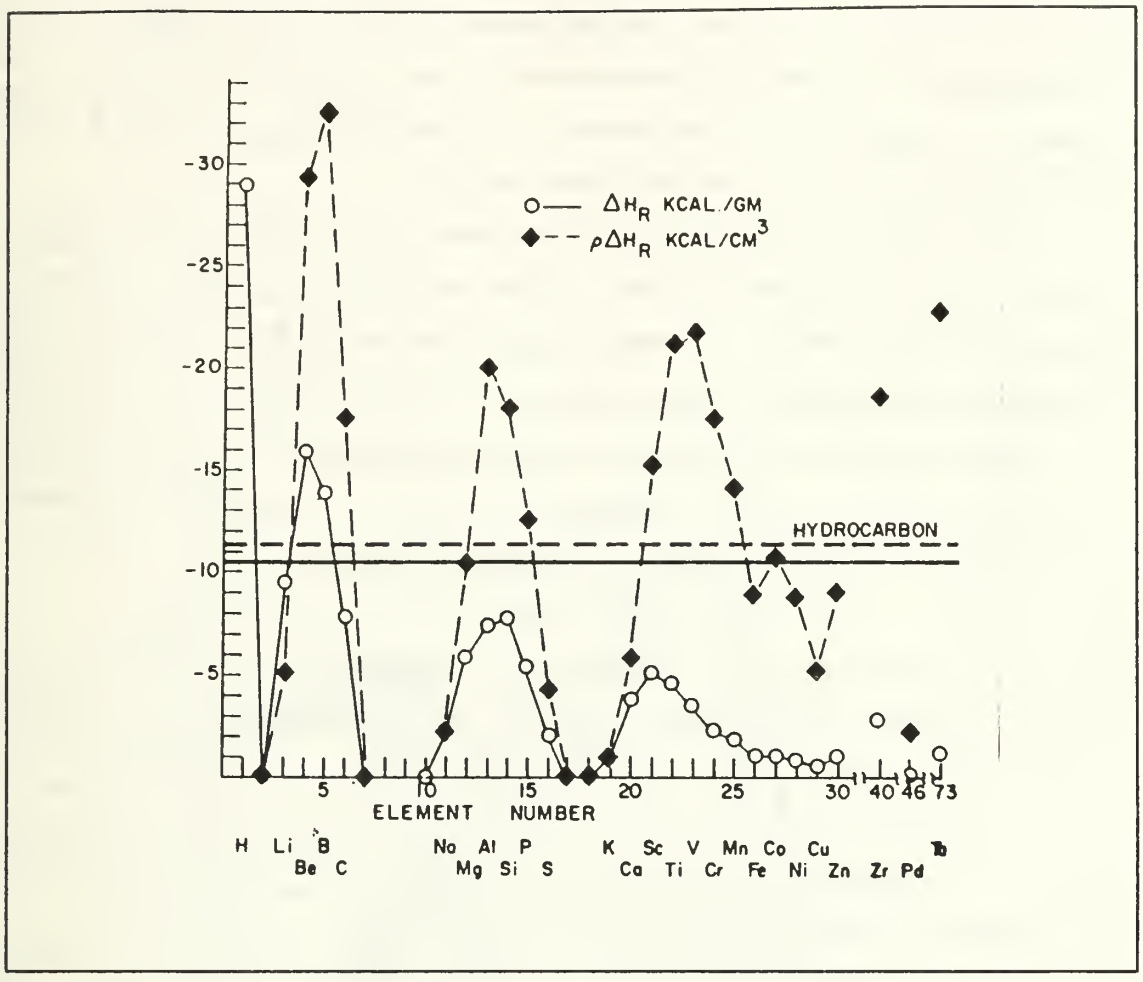

FIGURE 2: Heat of Combustion of Elements per Unit Mass and per Unit Volume. [Ref. 2:p. 161]

increased plume signature may negate much of the benefits of the performance gain obtained by the use of metal fuels. The magnitude of the increase in plume IR signature needs to be determined. Therefore, there is a strong need to both measure and effectively model the effects of metal additives on the infrared signature of ramjet powered missiles.

The plume infrared signature depends upon the plume temperature, optical properties of the gases and particles and the missile location and speed of motion. There are three basic categories of infrared signals, 1) spectral, 2) temporal, 3) spatial. Spectral refers to the wavelength dependence of the radiation. Temporal refers to the time varying nature

of the radiation and usually is effected by the source's motion. Spatial distribution depends on the viewed aspect of the source and usually remains constant at long distances. In this study, the primary interest was in the spectral emission. [Ref. 5:p. 57]

There are two basic types of emitters in the plume, solid bodies and gases. Unlike visible light, which is dependent upon the reflected wavelength, solid body infrared signals come mostly from emission (emitter temperature dependent) vice reflection. Solid components usually have a continuous power distribution across the wavelength spectrum and are referred to as continuum radiators (Figure 3). Gas radiation, however,

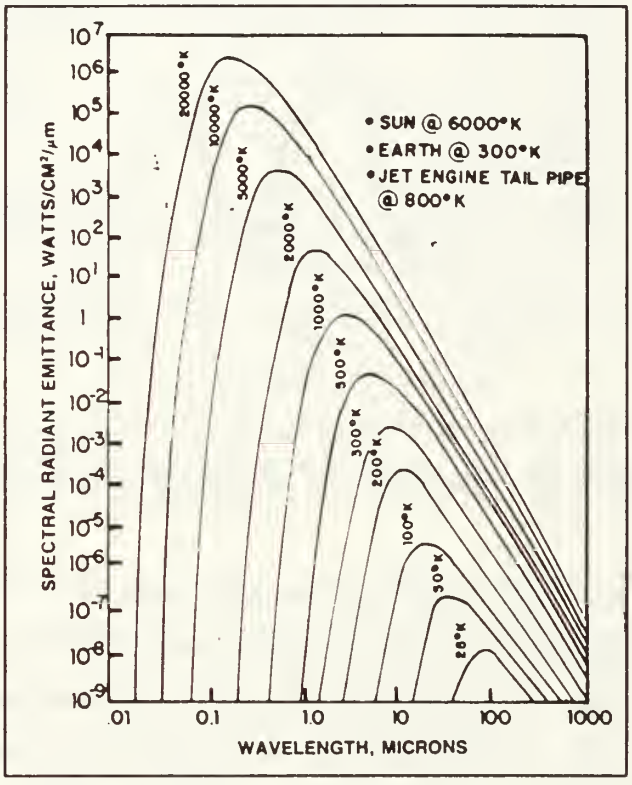

FIGURE 3: Spectral Radiant Emittance From a Black Body. [Ref. 4:p. 385]

depends upon both emission and scattering and tends to produce signals in discrete small bands across the spectrum. They are referred to as line radiators or emitters. [Ref. 4:pp. 382-389] The scattering of electromagnetic radiation by particles is generally divided into three

regions. Rayleigh scattering occurs when the particle size is small with respect to the wavelength of the illuminating beam. In this case, the photon flux is proportional to $1/\lambda^4$.

Mie scattering occurs when the particle size is approximately the same as the wavelength and the refractive index is significantly different from that of the scattering medium. This type of scattering can be used for modeling water droplets and plume particles. When particles become significantly larger than the wavelength of the illuminating beam, Mie scattering becomes indistinguishable from Fraunhofer diffraction. [Ref. 5:pp. 101-103]

The infrared signature of a missile comes primarily from hot parts on the airframe or propulsion system, reflected solar radiation, and radiation from the propulsion or plume gases and/or particles. Airframe heating becomes significant for supersonic missiles and primarily consists of emissions with wavelengths of 2-5 μm. Solar reflection occurs at wavelengths of 0.7-3.0 μm.

The plume has several complex interactions, including gas and particle interaction, shocks from external structures, reflected shocks due to pressure gradients and continued fuel combustion. These interactions are depicted in Figure 4. The signature of the plume gases is primarily caused by CO_2 and H_2O radiation, and has peaks at 1.4-1.9, 2.7, 4.3, 5-8, and 14-16 μm (Figure 5). In the plume the burning of residual motor H_2 and CO with ambient oxygen (termed afterburning) can contribute to the IR signature. The latter is known to be important for solid propellant rocket motors. However, for ramjets there is generally little H_2 and/or CO in the plume and little if any afterburning is expected. Metal particles added to the fuel to increase the Isp also contribute to the plume IR signature. Particles which are solidified as they leave the exhaust nozzle have low emittance and, therefore, should not contribute significantly to plume IR signature (although the visibility may be high). Liquid particulates generally have much higher emittances which increase with particle size.

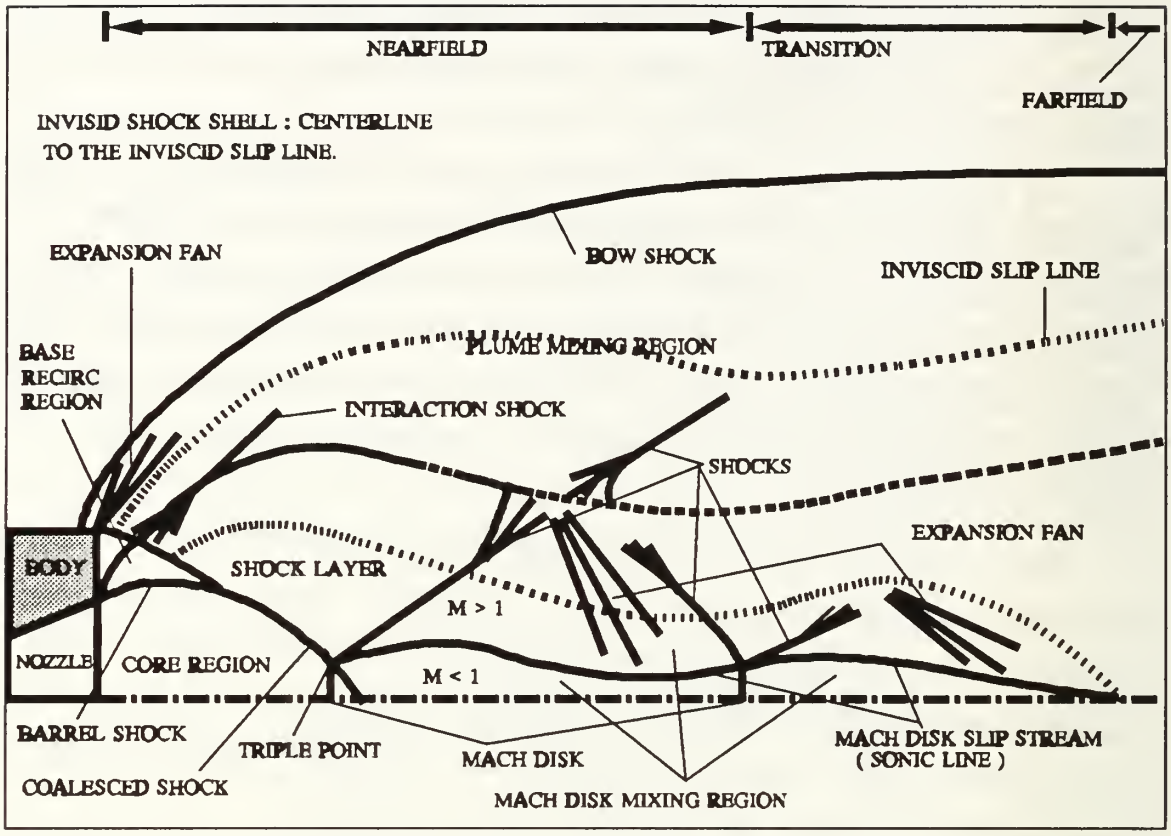

FIGURE 4: Exhaust Plume of a Conical Nozzle at Altitude with M_∞. (Adapted from [Ref. 6:p. 783 and Ref. 7:p. 9])

These particles can significantly affect the plume IR signature. Small particle (< 1μm) are generally in equilibrium with the gas. At ramjet exhaust temperatures these particles generally will be solids. Larger agglomerates of metals can form within the combustor. Depending upon the obtainable combustion efficiency, unburned large molten metal and metal oxides particles can pass from the combustor into the plume.

The plume emissions are reduced by atmospheric absorption (Figure 6) and by cooling of the gases through the mixing of air with the plume gases. [Ref. 4:p. 238-239, 382-389]

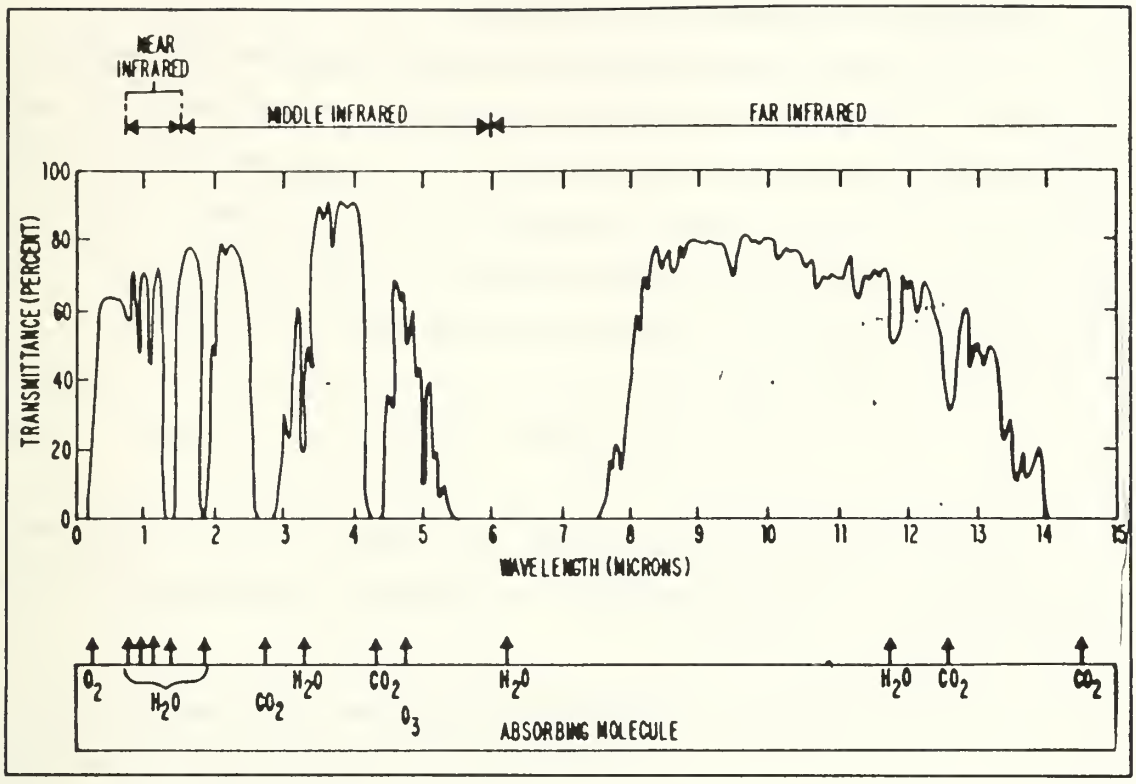

FIGURE 5: Atmospheric Attenuation of Infrared Radiation. [Ref. 4:p. 387]

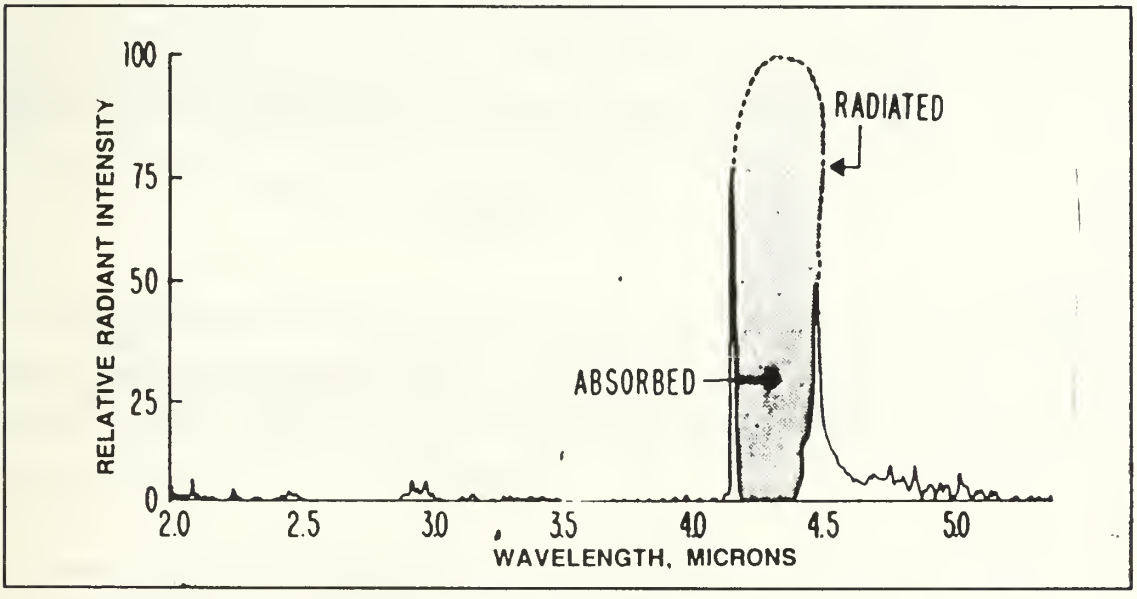

FIGURE 6: Exhaust Plume Infrared Radiation at 4.3 μm and the Absorption by the Atmosphere. [Ref. 4:p. 388]

B. OVERVIEW OF INFRARED RADIATION THEORY

The infrared (IR) spectrum covers electromagnetic emissions with wavelengths from 0.77 to 1000 μm. It can be broken into four general bandwidths, 1) near IR or short-wave IR, 2) midwave IR, 3) far IR, and 4) extreme IR. Figure 7 shows the range of each sub-area. Molecules and atoms which are excited above ground energies emit photons which are the IR energy carriers. The energy of the photon can be found by

$$E = h\,c\,/\,\lambda$$

When an infrared ray impacts an object it can be absorbed (α), reflected (ρ), or transmitted (τ). Kirchhoff's Law applies in all cases;

$$\alpha + \rho + \tau = 1$$

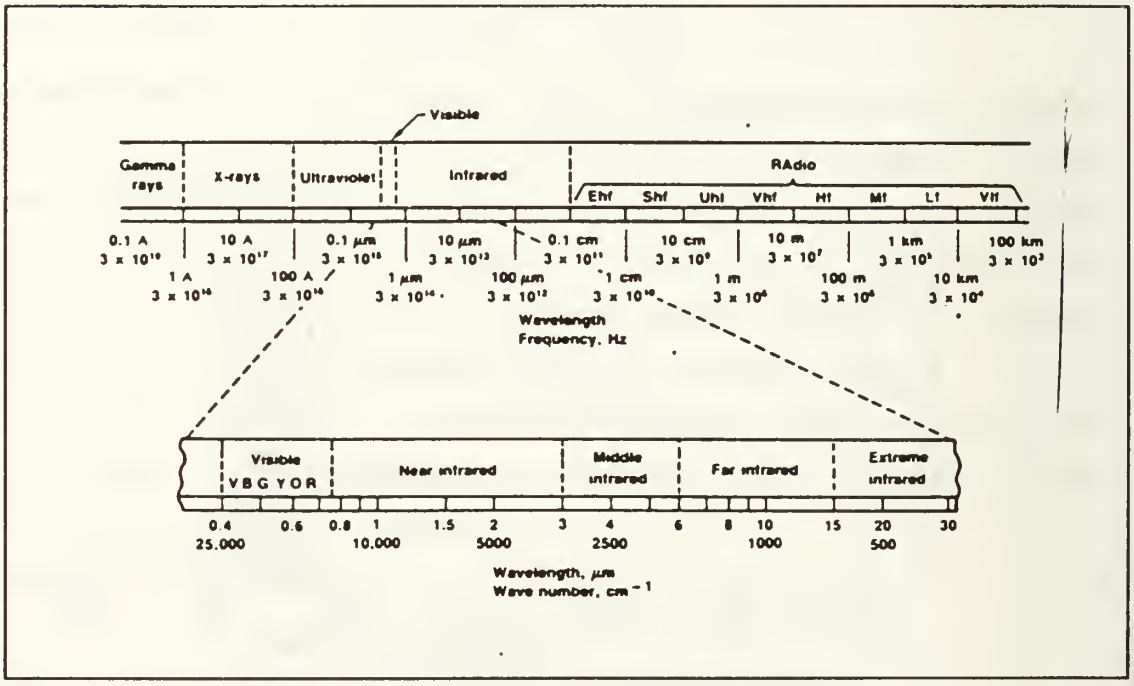

FIGURE 7: The Electromagnetic Spectrum [Ref. 5:p. 5]

In a case where $\alpha = 1$, then all the ray is absorbed and the body appears black. This body is referred to as a "black body". For a black body emitter, the radiant emittance (also known as radiancy, emissive power, or radiant exitance) is determined by the Stefan-Boltzmann Law.

$$M_b = \sigma T^4$$

Planck's Law shows how the photon wavelength and a black body emitter's temperature effect the radiant emittance.

$$M_b = \int_0^\infty M_{\lambda b} \, d\lambda$$

$$M_{\lambda b} = (2 \pi h c^2) / (\lambda^5 (e^{hc/\lambda kT} - 1))$$

The maximum black body spectral radiant emittance can be found by using Wien's displacement law (Figure 3);

$$\lambda_{max} = 2898/T \qquad (\mu m)$$

All other materials can be broken into two other categories, gray bodies and selective radiators. Emissivity (ε) is a comparison of their spectral radiant emittance to that of a black-body radiator.

$$M_\lambda = \varepsilon M_{\lambda b}$$

Gray bodies have a constant emissivity, while selective radiators have emissivities that are dependent on wavelength. For a black body, $\varepsilon = 1$. For gray bodies, emissivity can be used to compare radiant emittance. [Ref. 5:pp. 4-16]

The previous laws can also be written for photon intensity (N_λ), which is what several IR sensors measure. The photon intensity can be related to the spectral radiant emittance (Planck's Law) by;

$$N_\lambda = \varepsilon\lambda M_{\lambda b}/hc = \varepsilon 2\pi c/(\lambda^4(e^{hc/\lambda kT}-1)) \quad \text{(photons/sec m}^3\text{)}$$

For a black body, the Stefan-Boltzmann and Wein's laws can be modified to provide for photon intensity.

$$N_\lambda = 0.37\ \sigma\ T^3\ /\ k \quad \text{(photons/sec m}^2\text{)}$$

$$\lambda_{max} = 3663/T \quad [\mu m]$$

C. PURPOSE OF THESIS EFFORT

The objective of the thesis was to determine the effects of equivalence ratio (ϕ) and fuel composition on the infrared signature of solid fueled ramjets (SFRJ). Solid fuels investigated were Plexiglas, HTPB, and HTPB with aluminum, silicon, boron carbide, and/or magnesium. They were tested at chamber pressures of 80-170 psia and with equivalence ratios between 0.3 and 1.4. In addition to providing needed plume signature data for the SFRJ, this information can be used to validate numerical predictions from the SPF (Standardized Plume Flowfield) and SIRRM (Standardized Infrared Radiation Model) computer codes, which are used to predict the plume infrared signature.

II. EXPERIMENTAL APPARATUS

A. GENERAL SYSTEM LAYOUT AND INTERFACE

The testing was conducted at the Combustion Research Laboratory, Department of Aeronautics and Astronautics at the Naval Postgraduate School. The general layout of the system inside the cell is depicted in Figure 8. The high pressure air and auxiliary support gas systems can be seen in Figure 9. The system was remotely operated from the control room via a control panel and a 9836-S Hewlett-Packard computer. Main air was controlled by solenoid actuated, nitrogen operated ball valves with pressure regulated by a nitrogen controlled dome valve. All auxiliary gases were controlled by solenoid valves.

B. TEMPERATURE, PRESSURE, AND MASS FLOW RATE MEASUREMENTS

All temperatures were obtained using type K chromel/alumel thermocouples with Omega type K thermocouple extension wires. Pressures were obtained using Teledyne models 206-SA and 227-SA pressure transducers. Additional sensors included a water cooled thermocouple and water cooled pitot static tube for measurements within the plume.

The mass flow rates were determined using sonic nozzles together with measurements of stagnation pressures and temperatures. The system had five sonic nozzles, located in the lines of 1) main air, 2) the heater exit, 3) heater fuel (hydrogen), 4) heater oxygen, and 5) ignition fuel (hydrogen). Table I provides the sonic nozzle diameters and desired mass flow rates.

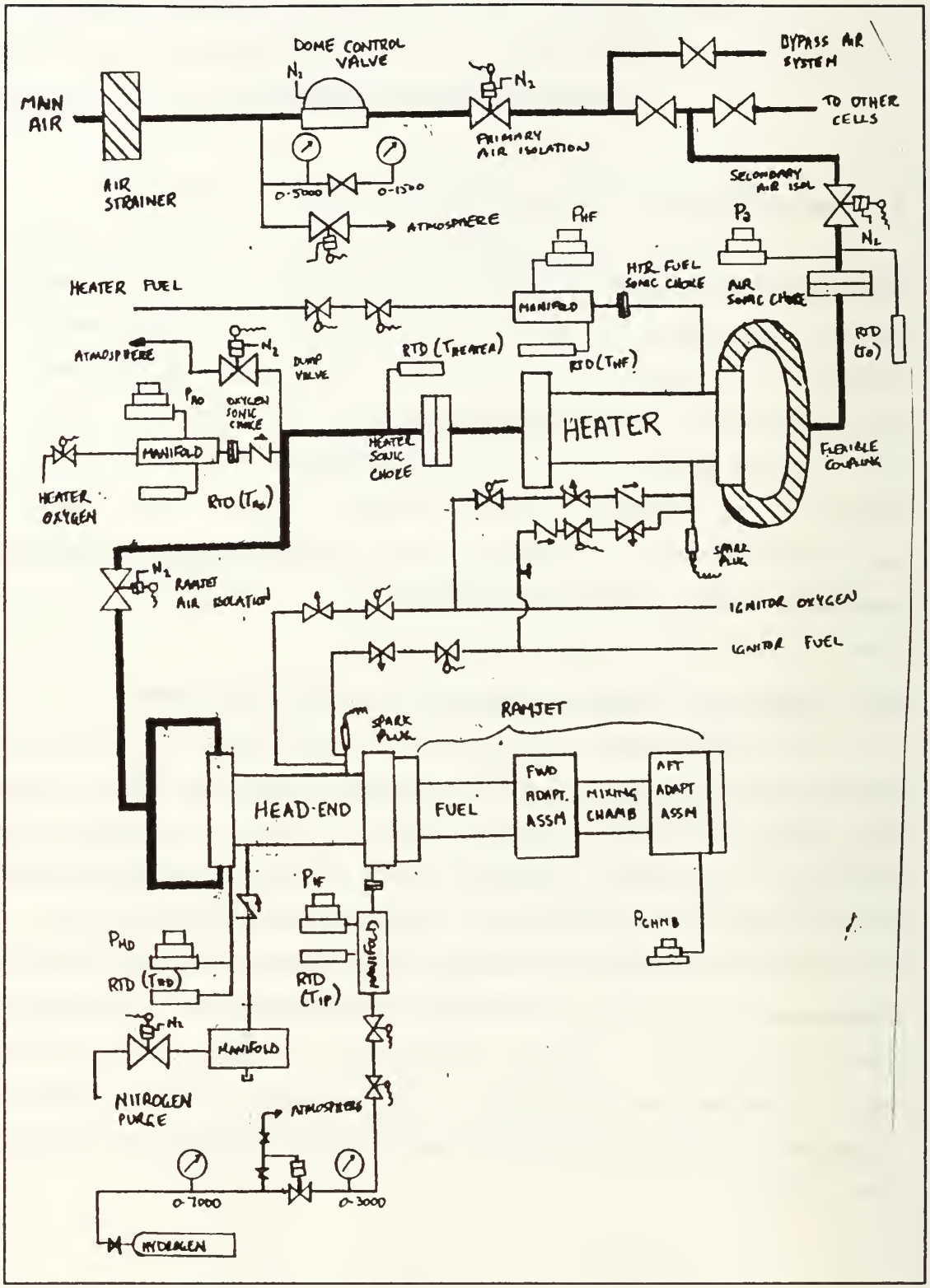

FIGURE 8: Test Cell Layout

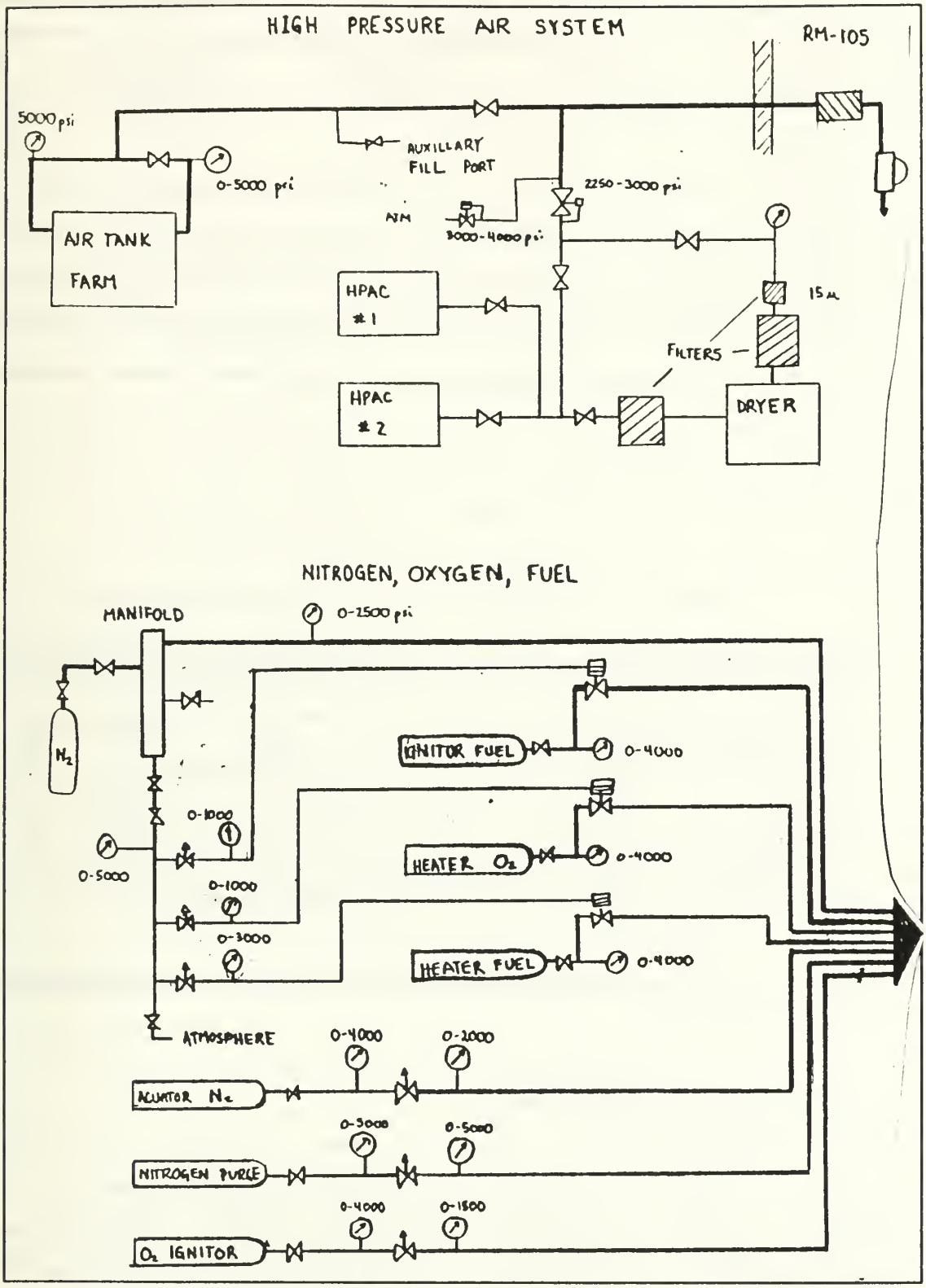

FIGURE 9: Auxiliary Systems Layout

TABLE I: SONIC NOZZLES AND MASS FLOW RATES

Location	Throat Diameter (in)	Minimum Pressure (psia)	Desired mass flow rate (lb_m/sec)
Main air	0.052	580	1.0
Heater inlet	0.607	225	1.0
Heater fuel	0.0395	465	0.0040
Heater O_2	0.052	540	0.0280
Ignit. fuel	0.040	400	0.0040

The mass flow rate at the throat (assuming the Mach number = 1), can be calculated by,

$$\dot{m} = C_D \, P_t \, A \, K \, / \, T_t^{1/2}$$

$$K = (\gamma \, MW/R)^{1/2} \, ((\gamma+1)/2)^{-[(\gamma+1)/(2(\gamma-1))]}$$

TABLE II: GAS CONSTANTS

Gas type	Molar wght	γ	R/MW	K
Air	28.97	1.40	53.3	0.53183
Oxygen	32.00	1.40	48.3	0.55888
Hydrogen	2.02	1.41	766.0	0.14067

C. DATA ACQUISITION EQUIPMENT

A Hewlett-Packard 3054-A Automatic Data Acquisition / Control System was used to control valve functions and time all test sequences. An AT computer utilized the Kaye Instruments DCALC program. This program was the controller for a MDAS 7000 data acquisition system. The MDAS has 16 card slots, each card can have up to ten channels and can record values up

to 9.22337 E+18 and as small as 5.42101 E-20. It is a sample-and-hold device with an average maximum sample rate of 80,000 channels/sec with pre-sampling and 185,000 channels/sec with no pre-sampling. [Ref. 8:p. 22]

D. INFRARED CAMERA SPECIFICATIONS

The AMEGA infrared camera has a series of filters and apertures, which can be used to look at specific spectral bands and/or temperature ranges. Major specifications for the AMEGA model 870 are given below.

1. Detector: SPRITE, thermoelectrically cooled MCT
   Mercury Cadmium Telluride sensor, operates at -70°C with 3 stage thermoelectric cooler.
2. Temperature Range: -20°C to 500°C (1500°C with filters)
3. Sensitivity: 0.1°C at 30°C
4. Accuracy: $\pm$ 2 % or $\pm$ 2°C
5. Wavelength: 2-5 μm
6. Lens: View range: 20°
   Min focus: 0.5 m
   Focal dist: 38 mm
   Geometrical Resolution: 3.5 mrad (50% contrast)
7. Control: CU-800C Computer system (TIC-8000 program)
8. Scan rate: 5.75 or 25 (in burst mode) full frames/sec
9. Aperture settings: 0 (5.8 mm), 1 (2.4 mm), and 2 (1.0 mm)
10. Filters: 0 (No filter), 1 (Glass), 2 (Flame)

[Ref. 9:pp. 1.2-1.3]

The camera measures in instrument units (IU) which are directly proportional to the photon intensity. The control program can then

convert the IU's to photon intensity and can use a simplified version of Planck's law to relate that intensity to absolute temperature.

$$I = R / (e^{B/T} - F)$$

Changing the aperture allowed for a larger range on the temperature scale. By adjusting the thermal control, this scale could be moved up and down. However, the maximum temperature eventually peaked, and increasing the voltage only reduced the scale by raising the minimum temperature. [Ref. 9:p. 8.2]

E. RAMJET MOTOR

The ramjet consisted of six components; the head-end, the fuel and casing, the forward adapter assembly, the mixing chamber, the aft adapter assembly, and the nozzle (Figure 10). The head-end assembly housed the igniter, several sensors, the nitrogen purge connection, the igniter fuel connection, and the step inlet. The reverse step generated a recirculation region at the head-end of the fuel grain. This provided the means for flame stabilization. It had an inner diameter of 0.75 inches. The gases rapidly expand into the cylindrical fuel grain and then pass through the forward adapter assembly. This assembly was made of 304 stainless steel. The assembly was 5.1 inches long and had an inner diameter that expanded from 1.4 to 2.2 inches. The mixing chamber was 8 inches long, had an inner diameter of 2.1 inches, and had a low carbon steel casing that housed a removable insulating (Dow Corning 93104) sleeve. It was threaded at both ends, which allowed the forward and aft adapter assemblies to be joined. The aft adapter assembly was also made of 304 stainless steel, had an inner diameter of 2.15 inches, was 4 inches long, and had the chamber pressure measurement connection. The flow finally passed through a converging-diverging nozzle. The nozzle

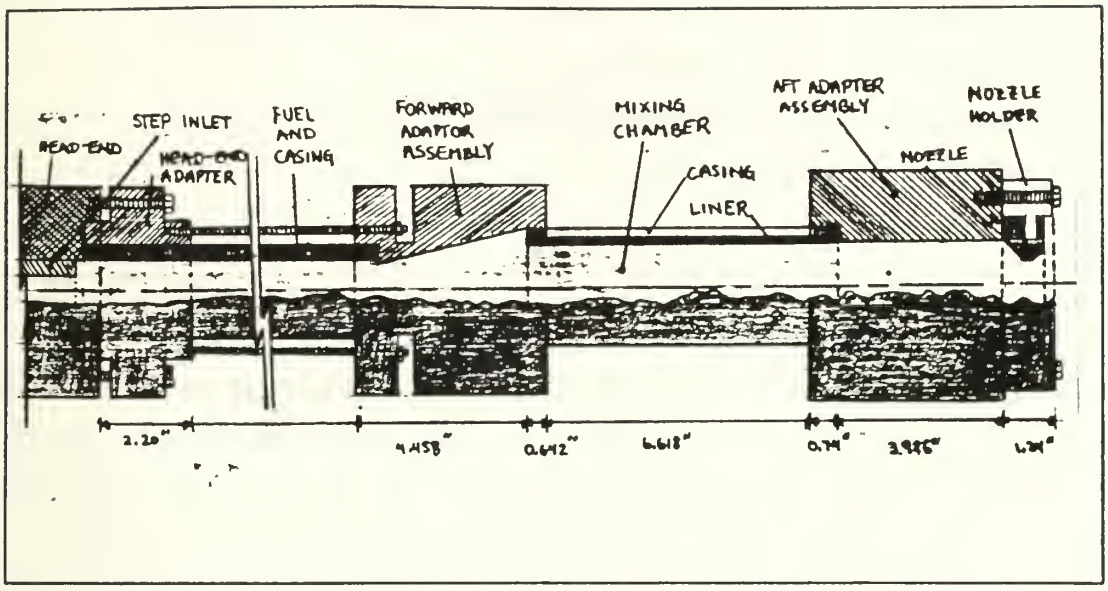

FIGURE 10: Ramjet Configuration

convergence had a half-angle of 45°, the divergence had a half-angle of 15°, and the throat had a flat of 0.1 inches. The throat was 1.17-1.30 inches in diameter and the nozzle exit diameter was 1.48-1.52 inches.

F. FUELS

Three basic fuel types were tested; Plexiglas, HTPB, and metalized HTPB. The cylindrical fuel grains had an inner diameter of 1.70-1.75 inches, a fuel thickness of 0.29-0.33 inches, and a length of either 6.5 or 13 inches. The metalized fuels were encased in an aluminum shell with a thickness of 0.65 inches. The Plexiglas fuels were manufactured at the Naval Postgraduate School. The metalized fuels provided by the Naval Weapons Center, China Lake, Ca., were M-096, M-096 (No Mg), M-103, M-014, M-105, and M-106. The actual fuel composition concentrations were classified. However, the major ingredients were as follows;

1. M-096(NM): HTPB, Boron Carbide, Catalyst
2. M-096: HTPB, Boron Carbide, Magnesium, Catalyst

3. M-103: HTPB, Boron Carbide, Aluminum, Catalyst

4. M-104: HTPB, Aluminum

5. M-105: HTPB, Aluminum, Catalyst

6. M-106: HTPB, Silicon

III. EXPERIMENTAL PROCEDURES

A. TEST PROCEDURE

1. Set Up

Initially, the five sonic nozzles were installed. Soot and combustion product residuals made it necessary that the igniter and lines to it were disassembled, cleaned, and reassembled for each test. The fuel was weighed and the length and inner diameter of both ends were measured and recorded. The fuel was then installed between the head-end adapter and forward assembly. The mixing chamber liner was inspected and replaced if required. Then the forward assembly, mixing chamber, and aft assembly were joined. If the nozzle had been used for a previous firing, the throat diameter was measured. When the metal fuels were used, significant nozzle erosion occurred. The nozzle was then reattached to the aft assembly to form the completed ramjet. The ramjet was attached to the head-end and all connections to the pressure transducers were made.

The infrared and video cameras were set up and covered with plastic if necessary. The infrared camera line-of-sight was placed perpendicular to the plume jet and at the same level as the nozzle exit. For the first 10 tests, the IR camera was placed four feet from the ramjet and centered at a location 11 inches downstream of the nozzle exit. For all other tests, the camera was placed five feet from the nozzle and focused at a location 15 inches downstream of the nozzle exit. This change was made to accommodate an increase in the distance of the plume thermocouples from the nozzle. The IR camera was focused by setting it to a zero aperture with no filter. Once it was properly focused, the aperture and filter were reset for the firing. For the tests 1-11, 18, 19, and 24, the camera was used with no filter and an aperture of two. For test 12, the aperture was changed to zero. For tests 13-17, the camera

was used with no filter and an aperture of one. For all other tests the glass filter was used with an aperture of one.

Various pressure and temperature measurement devices were placed in the plume. For tests 2-12, a water-cooled pitot static tube was installed for determining the plume Mach number. This instrument could become clogged and thus was removed when the metallized fuels were fired. A water-cooled thermocouple was installed for all tests from 2-24. A second thermocouple (not water-cooled) was installed between tests 8 and 9. For all tests prior to test 11, the instruments were located at 21 inches from the nozzle exit. All subsequent tests had the instruments moved to 25 inches from the nozzle exit. This was done so that the instruments remained in the subsonic flow.

The final portion of the setup required energizing the MDAS, HP and AT computers, the control panel, and the IR camera control systems.

2. Calibration and Calibration Checks

The pressure instruments were calibrated with a dead weight tester for the initial test, then once a week, or if the instrument provided faulty readings. In conjunction with the dead weight tester, the MDAS/DCALC system was used to obtain voltages from the pressure transducer subjected to a known pressure loading. With two different load data points, a linear relationship (slope and intercept) was obtained. These values were stored in the DCALC program for conversion of subsequent voltages directly to pressures. A similar method was used for calibrating the thermocouples. Prior to each test, the DCALC program was run to verify that all the thermocouples and pressure transducers were reading approximately ambient temperature and pressure, respectively.

3. Flow Rate Checks

Pre-firing flow rate checks were performed on main air, heater fuel, heater oxygen, and igniter fuel. The control and actuator nitrogen bottles were placed on-line and the main air isolation valve was opened. Each flow was then checked separately, by first placing the appropriate

supply bottle on line or, for the main air, the dome control valve was pressurized. A visual inspection was made to ensure that no one was in the cell and a warning alarm was sounded to ensure all personnel outside knew that the ramjet would have flow passing through it. The DCALC program was then executed and the flow was manually initiated from the control panel. The flow could subsequently be adjusted by raising or lowering the pressure setup point of the regulator.

4. Firing the Ramjet

Once the preliminaries were completed, the IR camera scale was selected for a range of 500°C, assigned to the virtual disk, and set for a 120-frame (approximately 20 seconds) sequential storage that was to be manually initiated. The HP computer control program was then started, so that the desired timing sequence could be input. This program controlled the solenoid operating valves and had four distinct time markers. These markers were 1) the time to flow air through the motor prior to ignition, 2) the total ignition time, 3) the burn time, and 4) the purge time. Normal values for these were 4, 1, 6, and 4 seconds, respectively. For the M-100 series fuel grains, the desired burn time was set to 5 seconds or less. After receiving the time markers, the program pauses until the actual firing starts.

Ambient pressure, read from a barometer, and temperature were recorded. All auxiliary bottles were then placed on line and the water flow to the plume instruments was started. A check was made to ensure that no personnel were downrange of the ramjet. A fire-warning alarm was then actuated. On the control panel, the safety keys were turned to "operate" and the main air was started. Initially the dump valve was open and the ramjet air isolation valve was shut (See Figure 8). The air flow discharged to the atmosphere through the dump valve after passing through the vitiated heater section. This allowed for the air to be pre-heated prior to firing. The heater gas flows were initiated and ignited. While the air temperature was rising, a video camera was started. When the air

temperature stabilized, the HP computer control, DCALC, and the IR camera programs were simultaneously executed. The HP program initiated the opening of the ramjet air valve and then closed the dump valve, redirecting the hot air through the ramjet. After the first time marker had elapsed, the fuel igniter actuated for the specified time. Main air flow continued until the preset burn time had expired, then it was redirected out the dump valve and a nitrogen purge was sent through the ramjet to extinguish the burning. The main air flow was maintained to cool the air heater. Once the heater had cooled, the main air flow was secured.

5. Post Firing Procedure

After the firing, the safety keys were turned off, the heater gases were stopped, the fire-warning alarm was secured, and the video camera was stopped. All auxiliary gas bottle isolations were shut. The IR camera data was reviewed and the necessary frames were transferred from the virtual disk to permanent storage. The DCALC data sheet was saved. The ramjet was then disassembled. The fuel was weighed and the inner diameters of both ends were measured.

B. DATA REDUCTION

The data analysis was performed with the DCALC program, the MICROPEP program [Ref 10], and a HP-28S calculator. The DCALC program provided the pressures, temperatures, and mass flow rates with respect to time. The MICROPEP program was used to provide the gas properties and theoretical adiabatic combustion temperature. Figure 11 depicts the station numbering. The parameters have sub-labels for indicating station numbers, and possibly a "p" for pre-ignition or "b" for during the burn.

1. DCALC Data

A pressure time trace was obtained to determine the actual burn time (t_b). The average mass flow rates of the heater fuel ($\dot{m}_h$), heater oxygen ($\dot{m}_{ox}$) and main air ($\dot{m}_o$) were obtained. These were combined to get

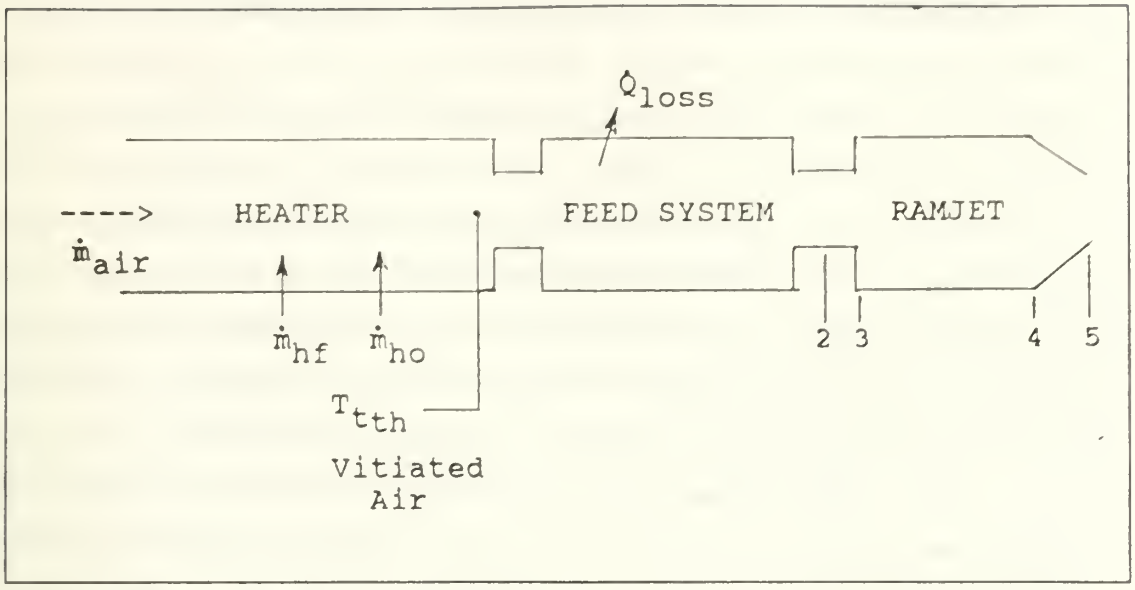

FIGURE 11: Data Reduction Stations

the total gas mass flow rate.

$$\dot{m}_g = \dot{m}_a + \dot{m}_{fx} + \dot{m}_c$$

Also, from the data sheet, the head-end pressures (P_{t2p} and P_{t2b}), chamber pressures (P_{4p} and P_{4b}), and head-end temperatures (T_{t2p} and T_{t2b}) were obtained.

The fuel mass flow rate ($\dot{m}_f$) was obtained by dividing the change in mass by the burn time. Adding all the mass flow rates together provided the total mass flow rate ($\dot{m}_{total}$). The fuel-air ratio was found by dividing the mass flow rate of the fuel by the gas mass flow rate ($f = \dot{m}_f/\dot{m}_g$) and the equivalence ratio was found by dividing the fuel-air ratio by the stoichiometric fuel air ratio.

$$\phi = f \; / \; f_{stoich}$$

2. Pre-Ignition Calculations

The pre-ignition data were used to determine two parameters, the air heat of formation (to account for heat losses between the air heater

and ramjet inlet) and the nozzle discharge coefficient (C_D). During this portion of the data analysis, $\dot{m}_f$ was zero. Air at 25°C has a heat of formation of zero. Using the pre-ignition head-end pressure (P_{t2p}), the mass flow rates of the gases, and guessing an approximate heat of formation for air, MICROPEP was used to calculate an expected head-end temperature. This temperature was compared to the actual head-end temperature (T_{t2p}). Then the air heat of formation was modified until the MICROPEP temperature and the head-end temperature matched. This heat of formation was used in all subsequent MICROPEP calculations.

The nozzle discharge coefficient (C_D) was used to determine an "effective" throat area. This coefficient also accounted for inaccuracies in the measurement of the nozzle diameter, pressures, temperatures, and heat losses. C_D was considered to be constant throughout the test. The following assumptions were made for the hot air flowing through the ramjet <u>prior</u> to ignition:

$$T_t = T_{t4p} = T_{t5p} = T_{t2p} = T_{2p}$$

$$MW = MW_{4p} = MW_{5p} \qquad P_{t4p} = P_{t5p}$$

$$\dot{m}_g = \dot{m}_{4p} = \dot{m}_{5p} \qquad \gamma = \gamma_{4p} = \gamma_{5p}$$

A pre-ignition molecular weight (MW_{4p}) and specific heat ratio (γ_{4p}) were obtained by running MICROPEP using the pre-ignition chamber static pressure (P_{4b}) and the mass flow rates of the gases. The nozzle contraction area ratio was known. For a throat Mach number of 1 the contraction area ratio yielded the pre-ignition chamber Mach number (M_{4p}). This Mach number was then used to solve for the chamber stagnation pressure (P_{t4p}) from the measured value of P_{4b}.

$$A_4/A_5 = [1/M_{4p}]\ [2/(\gamma+1)]\ [1+(\gamma-1)M_{4p}^2/2]^{(\gamma+1)/2(\gamma-1)}$$

$$P_{t4p} = P_{4p}[1+(\gamma-1)M_{4p}^2/2]^{\gamma/(\gamma-1)}$$

C_D was then found by applying the continuity equation.

$$C_D = \dot{m}_g \; / \; \{P_{t4p} A_5 \; [(\gamma g_c MW)/(R\ T_{t2p})]^{1/2} [2/(\gamma+1)]^{(\gamma+1)/2(\gamma-1)} \}$$

3. Combustion Efficiency Calculation

The next step was to calculate the temperature rise combustion efficiency (η). MICROPEP was run using the burning chamber pressure (P_{4b}) with all the gas and fuel flow rates to find values for the molecular weight (MW_{4b}), equilibrium chamber temperature (T_{4b}) and specific heat ratio (γ_{4b}). In the equations that follow, $\gamma = \gamma_{4b}$, $MW = MW_{4b}$, and γ is the "process" γ between A_4 and A_5.

$$\dot{m}_{total} = P_{4b}\ A_4\ M_{4b}\ [\gamma\ g_c\ MW\ /\ R\ T_{4b}]^{1/2}$$

These values were used to find the Mach number, M_{4b}. With this Mach number, the stagnation pressure could be found using the isentropic relationship.

$$P_{t4b} = P_{4b}\ [1 + (\gamma + 1)\ M_{4b}^2\ /\ 2]^{\gamma/(\gamma - 1)}$$

Using P_{t4b}, MICROPEP was rerun to find the <u>theoretical</u> stagnation temperature ($T_{t4b,th}$), and new values for the molecular weight (MW_{4b}) and specific heat ratio (γ_{4b}).

With the previous value of C_D, the experimental stagnation temperature (T_{t4exp}) was found using

$$\dot{m}_{total} = C_D\ P_{t4b}\ A_5\ \ [(\gamma\ g_c\ MW)/(R\ T_{t4exp})]^{1/2}\ \ [2/(\gamma+1)]^{(\gamma+1)/2(\gamma-1)}$$

With these temperature values, the combustion efficiency was calculated using

$$\eta = (T_{t4exp} - T_{t2b}) / (T_{t4b,th} - T_{t2b})$$

The combustion efficiencies for the metalized fuels were classified. In order to include these values, all the values of η were normalized with a reference value (η_{ref}).

4. Fuel Regression Rate

The average fuel regression rate ($\dot{r}$) was obtained by first calculating the post-firing average inner diameter ($d_{f\ ave}$). The value of $d_{f\ ave}$ was calculated using the change of mass (Δm) given by

$$\Delta m = \rho_{fuel} L_{fuel} \pi (d_{f\ ave}^2 - d_{i\ ave}^2)/4$$

With the $d_{f\ ave}$ known, the average fuel regression rate was calculated using

$$\dot{r} = (d_{f\ ave} - d_{i\ ave}) / (2\ t_b)$$

5. Emissivity of the Plume

The plume temperatures produced by the IR camera depend upon the specified emissivity (ε_o). The equivalent plume emissivity at a point within the subsonic region of the plume was determined by adjusting ε_o until the calculated plume temperature was identical to the measured plume static temperature. It was assumed that the plume was a gray body. The camera control software allowed for the insertion of an emissivity between 0.1 and 1. As ε_o was decreased the plume temperature increased. The actual maximum temperature was often above the maximum temperature permitted by the IR camera for the specified filter and aperture setting. In this case, it was necessary to use a modified version of Planck's Law

to get ε_o. The process consisted of four steps; calculating the plume Mach number and effective γ, determining the actual plume static temperature, obtaining an average IR camera plume temperature in the same location as the probes and then using Planck's Law to find the ε_o.

In order to obtain the emissivity of the gas-particle mixture, it was assumed that the particles and gases were at the same temperature. A pitot static pressure tube and thermocouples were installed into a subsonic portion of the plume. The plume stagnation temperature ($T_{t\ plume}$), stagnation pressure ($P_{t\ plume}$), and static pressure (P_{plume}) were then obtained from the DCALC data sheet. An energy balance was then used to determine an effective specific heat ratio of the plume(γ_{plume}). An approximate energy balance was used to determine the entrained air mass flow rate in the plume ($\dot{m}_a$). The specific heats at constant pressure for the air and plume were assumed to be equal, thus simplifying the energy balance.

$$(\dot{m}_{total}+\dot{m}_a)T_{t\ plume} = \dot{m}_{total}T_{t4b} + \dot{m}_a T_{amb}$$

Mass averaging the specific heat ratios then provided an "effective" specific heat ratio for the plume, namely

$$\gamma_{plume} = (\gamma\dot{m}_a + \gamma 4b\ \dot{m}_{total})/(\dot{m}_a + \dot{m}_{total})$$

The isentropic pressure relationship was then used to find the plume Mach number (M_{plume}). The Mach number and either the water-cooled or non-water-cooled thermocouple temperature ($T_{tc\ plume}$ or $T_{t\ plume}$; 'c' indicates water cooled) were used to find the static temperature with the isentropic temperature relation. This value was not highly accurate since the temperature measurements were not corrected for radiation.

The IR camera computer program allowed for a "spot" or "area" function to be used to determine the plume temperature. Both functions were used to observe the IR calculated temperature around the probe. For

the object emissivity calculations, the "area" statistical plume temperatures for 4-6 frames were averaged to obtain the average camera plume temperature ($T_{cam\ ave}$). Knowing that the camera captured signal was independent of the object emissivity, it was determined that [Ref. 9:pp 8.1-8.2],

$$I = R / (e^{B/Tcam\ ave} - F) = \varepsilon_o R / (e^{B/Tprobe} - F)$$

Thus,

$$\varepsilon_o = (e^{B/Tprobe} - F) / (e^{B/Tcam\ ave} - F)$$

In the equation above, B and F are functions of the camera filter and aperture and are shown in Table III.

TABLE III: EMISSIVITY CORRECTION FACTORS

Filter	Aperture	B	F
None (NOF)	0	3146	-438
None	1	3286	-116
None	2	3513	-4.94
Glass	1	2935	-3.58

[Ref. 9:p 8.2]

IV. RESULTS AND DISCUSSION

A. RAMJET FIRING RESULTS

Twenty-four tests were completed and the results are consolidated into Tables IV through VII. The IR data are provided in Appendix A.

1. General Comments Concerning the Tabulated Results

1. If a block contains an "X", that information was not available.

2. The combustion efficiencies were classified for all the metalized fuels. The efficiencies for all the tests have been normalized with a reference value of efficiency.

3. During test 7 the water-cooled thermocouple was overheated. This instrument subsequently provided low plume temperatures and was not included in the tables after test 8. ε_o was calculated using the non-water-cooled probe temperature when it was available.

4. The irradiance/emittance values are based on an object emissivity equal to 1 (a black body approximation).

5. For tests 20-23 a glass filter was used, while all other tests used no filter. The glass filter attenuates the signal (the data on the actual percent attenuation versus wavelength was unavailable). However, the system software included the calibration curves for all apertures and filters. This permits all data to be compared on an absolute basis.

2. Specific Comments About Individual Tests

1. Test 1: This test was performed without the IR camera. The fuel never ignited and, therefore, the data were not included.

2. Test 2: IR data were lost.

3. Test 3: A communication error occurred between the MDAS and DCALC program, therefore no DCALC data were available. This test run was included because of the irradiance data.

4. Test 4: This was a previously fired M-096 fuel. A programmed three second burn time was too much and a fuel casing rupture occurred. These data were excluded, however M_{plume} = 0.45.

5. Test 5: The MDAS data were not obtained due to operator error.

6. Test 8: The IR data were not obtained due an improper setup by the operator of the sequence storing routine.

7. Test 9: A hold-down leg was left unlocked to allow for the plume instruments to be aligned with the nozzle exit. Upon ignition the plume instrument was turned sideways, negating the plume temperature data.

8. Test 10: The grain was initially fired and no IR or visual data were noted, even though the fuel ignited. Based on the lack of both the IR and visual data, it was assumed that the fuel had not ignited. After cooling the ramjet, the test was run again. Approximately 1.5 seconds after ignition the casing rupture. The data were discarded with the exception of the value for M_{plume}, which was equal to 0.7.

9. Test 13: The IR data were lost due to turning off the computer prior to transferring the data off of the virtual disk.

10. Test 15: A casing failure occurred near the very end of the run due to an excess programmed burn time. Also a communication error caused the DCALC data to be lost.

11. Test 17: A casing failure occurred near the very end of the run due to an excessive programmed burn time. Since this occurred in the final second of the test, a weight correction was made to account for the missing casing. These data can be compared with those of Test 24.

12. Test 20: The M-104 thrust was greater than anticipated and forced the plume instruments out of the plume. For subsequent tests the instrument table was weighted down.

3. Plume Mach Number and Specific Heat Ratio

The first ten tests were used to determine the approximate Mach number (M_{plume}) and the effective plume specific heat ratio (γ_{plume}) at 15 nozzle exit diameters into the plume. These values were then used to find

T_{plume}. M_{plume} varied from 0.45-1.05. For test 4, which used a metalized fuel, the calculated low Mach number was probably due to particles clogging the pitot tube. Tests 6 and 7 showed Mach numbers greater than one, however the stagnation pressure read one psia greater than the static pressure with no flow, making these values questionable. The stagnation pressure transducer was replaced with one that had a smaller range, and then both the static and stagnation pressure transducers were recalibrated for tests 9-12. Disregarding tests 7 and 8, all other tests indicated that the plume Mach number was approximately 0.7.

An energy balance was used to determine the amount of ambient air that was mixed with the plume products at the point of temperature measurement. The ambient air mass flow rate to exhaust mass flow rate was found to be about 3 to 1 for all the tests. The mass-averaged specific heat ratio was found to be 1.34-1.38.

For tests 13-24, the plume was assumed to have M_{plume}=0.7 and γ_{plume}=1.35.

4. Plume Temperature

For tests 2-24, a water-cooled thermocouple was used to measure the actual plume temperature. During test 7, this thermocouple was overheated. An instrument calibration check showed that it was operating properly, however the water cooling sleeve had an unrepairable leak. This leakage lead to excessive cooling of the sensor wire. Another non-water-cooled thermocouple was installed prior to test 9. This instrument consistently read higher, from 50-500°R, than the water cooled thermocouple. For tests 11-24, the non-water-cooled instrument was used to find the plume temperature.

5. Emissivity

Both the T_{plume} and $T_{cam\ ave}$ were obtained for the same period after ignition. This required the DCALC and IR data times to be synchronized (manually after the test). A representative frame was selected from the IR data and the time elapsed between it and the initial IR frame was

found. Then the $T_{cam\ ave}$ was found by averaging the temperature around the probe for 4-6 frames. The temperatures were obtained using the "area" and "stat" functions for the IR system. The DCALC T_{plume} versus time trace was then checked to find the average T_{plume} for the same period. These temperatures were then used to find the average emissivity. The emissivities varied from 0.07-0.39, neglecting the results from test 7. The average plume emissivity for all the fuels was approximately 0.2. Much of the variation in the calculated plume emissivity could have resulted from the inaccuracy of the plume temperature measurements. The response times of the thermocouples were too long and no radiation corrections were made. Future measurements should use much finer thermocouple wire mounted within radiation shielding enclosures. Based upon other experiments being conducted at the Combustion Laboratory, it was expected that the effective plume emissivity was below 0.10. If true, this would indicate that the thermocouples did not record the actual maximum temperatures.

6. The Effects of Fuel Composition, ϕ and η on Irradiance

The irradiances/emittances provided were obtained by modeling the plume as a black body. The camera temperature range (difference between the maximum and minimum temperatures) was restricted to a maximum of 500 degrees, which was significantly less than the temperature range within the plume. This meant that only a portion of the plume temperature could be monitored. The camera aperture and filter were set prior to the firing based on an expected intensity/temperature of the plume. The aperture and filter were manually controlled on the camera and could not be changed once the firing began. Another means for adjusting the IR camera was the thermal level control that allowed for partial movement of the 500 degree band up and down the temperature scale. However, the program still restricted the maximum temperature based on the filter and aperture selected, and the burn times between 5-8 seconds were inadequate to permit readjustment.

In order to obtain data for the plume emissivity the temperature band was kept low on the temperature scale, which often lead to signal saturation at the center of the plume. This has been annotated by a ">" sign or if excessive saturation, a ">>" sign in Tables IV through VII.

After the emissivities were determined, attempts were made to obtain adjusted irradiances. The object irradiance is calculated in the software from the camera signal, accounting for atmospheric absorption and reflected irradiance. With an ε_o=1, the object signal matches the camera signal. Since the actual camera signal was a constant, lowering the specified ε_o caused the object irradiance to decrease and the temperature to increase. Therefore, the actual irradiance of the object is less than what is shown in Tables IV to VII. Also when the ε_o was adjusted, the saturated region increased in size. In order to compare results, the value of ε_o was kept at one for all the tests.

Since IR signature is very sensitive to temperature it was expected that the irradiance might correlate with the actual combustor stagnation temperature ($T_{t4\ exp}$). $T_{t4\ exp}$ increases as the equivalence ratio approaches unity. It is also affected by the fuel composition and by the obtainable combustion efficiency. The measured irradiances for ε_o=1.0 are plotted vs $T_{t4\ exp}/T_{ref}$ in Figure 12. This figure is typical of what might be expected from a field instrument which would also use a fixed value for ε_o. The actual values of irradiance will be lower (since ε_o<1.0) and the relative values between the fuels may be somewhat different due to differences in the actual ε_o values from test to test.

As expected, increasing $T_{t4\ exp}$ increased the irradiance. The irradiance increased approximately with the second power of the actual combustor stagnation temperature. Also from Figure 12, some limited data trends were noted. The addition of magnesium caused the irradiance to increase. The addition of silicon caused the irradiance to decrease. The use of B_4C with Al (M-103 fuel) appears to have greatly increased the plume irradiance. Comparison of the calculated exhaust species for the high

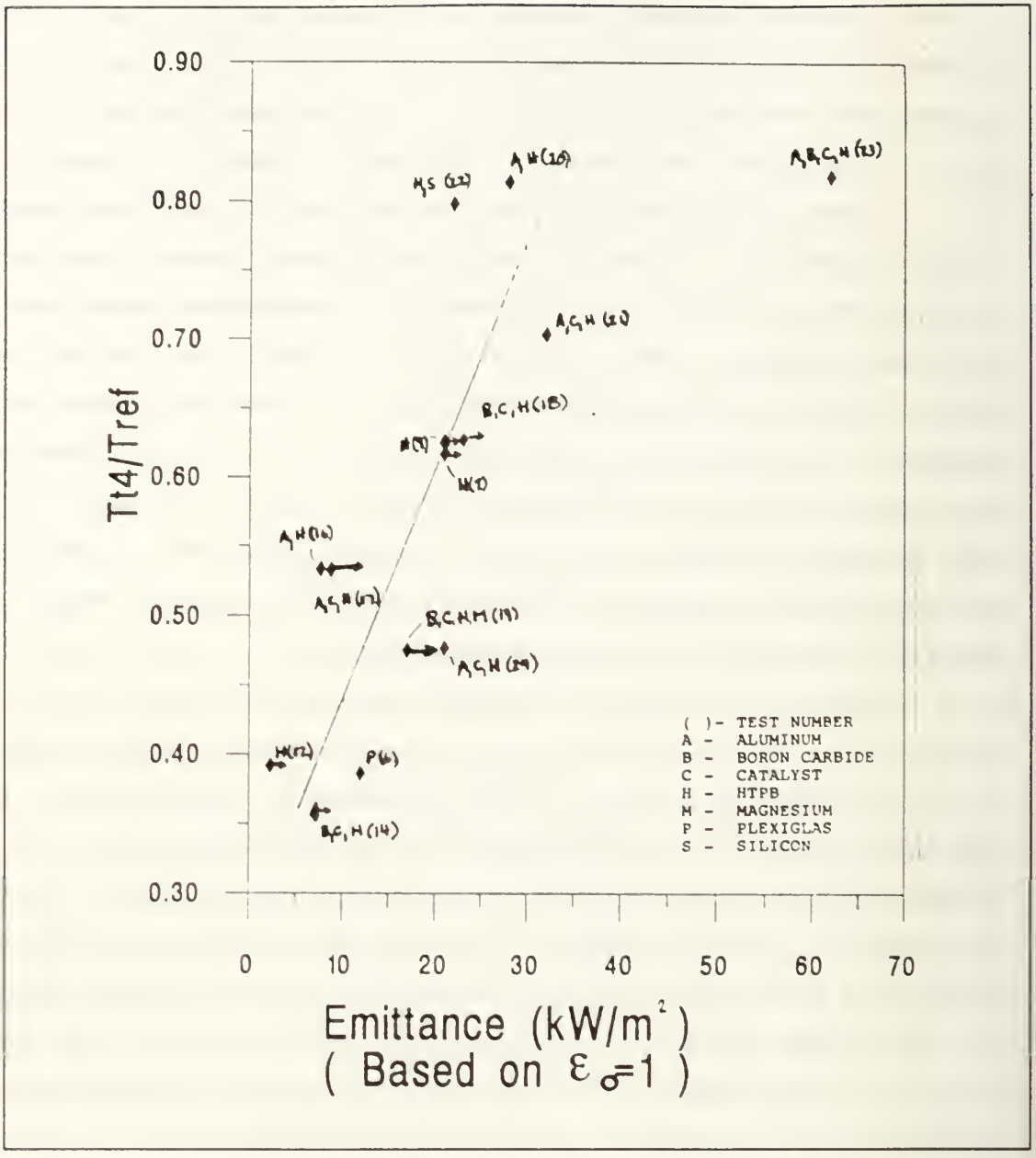

FIGURE 12: Irradiance Characteristics with T_{t4}

temperature data using M-104 and M-103 fuels indicated that significant amounts of BHO_2 were present in the exhaust of the M-103 test. However, this was based on very limited data and the effect was not present at lower temperatures. Finally it can be seen that the metallized M-096 fuel and pure HTPB had similar IR signatures in the 2-5 μm.

TABLE IV: RESULTS FROM TESTS 2-8

Test No.	Units	2	3	6	7	8
Fuel Type		PLEX	HTPB	PLEX	HTPB	HTPB
L_{fuel}	inch	11.88	13.00	11.94	12.06	13.00
P_{amb}	psia	14.62	14.53	14.19	14.53	14.53
T_{amb}	°R	524.9	524.9	524.9	524.9	520.1
d_{th}	inch	1.22	1.22	1.22	1.22	1.23
Filter		NOF	NOF	NOF	NOF	NOF
Aperture		2	2	2	2	2
D_{cam}	inch	48	48	48	48	48
L_{probe}	inch	21	21	21	21	21
P_{4b}	psia	87.5	X	91	107	118
T_{t2b}	°R	897	X	1126	1153	1.13
$\dot{r}$	in/sec	0.0174	0.0331	0.0375	0.0263	0.0312
$\dot{m}_f$	lbm/sec	0.0025	X	0.0041	0.0041	0.0039
$\dot{m}_{ox}$	lbm/sec	0.0318	X	0.0285	0.0287	0.0321
$\dot{m}_o$	lbm/sec	0.9850	X	1.0095	0.9250	0.9990
$\dot{m}_t$	lbm/sec	0.0538	X	0.0985	0.0826	0.0861
ε_c	sec	6.20	7.00	7.35	6.70	9.55
Φ		0.44	X	0.79	1.18	1.13
η/η_{ref}		0.74	X	0.88	0.84	0.88
$T_{cam\ max}$	°R	X	>1387	1226	>1412	X
$T_{cam\ ave}$	°R	X	1248	793	1183	X
$T_{tc\ plume}$	°R	1550	X	1080	1480	~~950~~
$T_{t\ plume}$	°R	X	X	X	X	X
M_{plume}		0.7	X	~~1.1~~	~~1.05~~	0.7
γ_{plume}		1.336	X	1.368	1.359	1.368
ε_c		X	X	0.20	~~0.50~~	X
M_t (ε_c=1)	W/m²	X	>20000	12000	>21000	X

(Lined out data were found not to be valid.)

TABLE V: RESULTS FROM TESTS 9-14

Test No.	Units	9	11	12	13	14
Fuel Type		HTPB	HTPB	HTPB	M096 (NM)	M096 (NM)
L_{fuel}	inch	13.00	6.13	6.44	6.38	6.5
P_{amb}	psia	14.53	14.66	14.71	14.72	14.73
T_{amb}	°R	521.7	524.8	515.9	515.9	521.0
$\dot{m}_h$	inch	1.23	1.23	1.23	1.24	1.24
Filter		NOF	NOF	NOF	NOF	NOF
Aperture		2	2	0	1	1
D_{cam}	inch	48	60	60	60	60
L_{probe}	inch	21	25	25	25	25
P_{4b}	psia	122	89	88.5	90	87
T_{t2b}	°R	1085	1084	1077	1128	1138
$\dot{r}$	in/sec	0.0305	0.0291	0.0262	0.0276	0.0272
$\dot{m}_h$	lbm/sec	0.0040	0.0040	0.0040	0.0044	0.0044
$\dot{m}_{ox}$	lbm/sec	0.0313	0.0308	0.0291	0.0312	0.0313
$\dot{m}_o$	lbm/sec	1.0350	1.0070	1.0130	1.0200	1.0200
$\dot{m}_f$	lbm/sec	0.0782	0.0358	0.0339	0.0561	0.0564
t_b	sec	9.30	7.20	8.00	7.50	7.50
Φ		1.07	0.47	0.44	0.56	0.54
η/η_{ref}		0.84	0.75	0.77	0.50	0.56
$T_{cam\ max}$	°R	>1412	X	>805	X	>1075
$T_{cam\ ave}$	°R	1187	X	685	X	821
$T_{t\ plume}$	°R	X	1077	1070	1210	1200
M_{plume}		0.70	0.85	0.70	X	X
γ_{plume}		1.373	1.368	X	X	X
ε_o		X	X	0.17	X	0.22
M_b (ε_o=1)	W/m^2	>21000	X	>2271	X	>7224

TABLE VI: RESULTS FROM TESTS 15-19

Test No	Units	15	16	17	18	19
Fuel Type		M104	M104	M105	M096 (NM)	M096
L_{fuel}	inch	6.44	6.47	6.50	13.06	13.00
ε_{e} .	psia	14.71	14.56	14.71	14.65	14.69
T_{amb}	°R	521.0	521.0	524.9	524.9	521.7
d_{th}	inch	1.24	1.24	1.24	1.27	1.30
Filter		NOF	NOF	NOF	NOF	NOF
Aperture		1	1	1	2	2
D_{cam}	inch	60	60	60	60	60
L_{probe}	inch	25	25	25	25	25
P_{4b}	psia	X	102	105	120	107
T_{t2b}	°R	X	1132	1149	1077	1080
$\dot{r}$	in/sec	X	0.0324	0.0348	0.0277	0.0332
$\dot{m}_{h}$	lbm/sec	X	0.0042	0.0043	0.0039	0.0040
$\dot{m}_{ox}$	lbm/sec	X	0.0307	0.0307	0.0321	0.0310
$\dot{m}_{o}$	lbm/sec	X	1.0200	1.0220	0.9960	1.0170
$\dot{m}_{f}$	lbm/sec	X	0.0747	0.0829	0.1134	0.1353
t_{b}	sec	X	6.35	6.20	6.35	5.55
Φ		X	6.35	0.33	1.12	1.31
η/η_{ref}		X	0.74	0.72	0.80	0.55
$T_{cam\ max}$	°R	1130	1129	>>1091	>1444	>>1412
$T_{cam\ ave}$	°R	<852	825	1012	1223	1217
$T_{t\ plume}$	°R	X	1430	1550	2000	2160
ε_{o}		X	0.14	0.39	0.20	0.16
M_{b} (ε_{o}=1)	W/m^2	8759	8761	>>7651	>23000	>>21000

TABLE VII: RESULTS FROM TESTS 20-24

Test No	Units	20	21	22	23	24
Fuel Type		M104	M105	M105	M103	M105
L_{fuel}	inch	12.94	13.00	13.07	12.94	6.47
P_{amb}	psia	16.14	16.12	16.11	14.66	14.65
T_{amb}	°R	530.0	524.6	524.6	524.6	523.1
d_{th}	inch	1.17	1.22	1.25	1.30	1.30
Filter		GLS	GLS	GLS	GLS	NOF
Aperture		1	1	1	1	2
D_{cam}	inch	60	60	60	60	60
L_{probe}	inch	25	25	25	25	25
P_{4b}	psia	173	147	137	125	91
T_{t2b}	°R	1104	1064	1104	1133	1131
$\dot{r}$	in/sec	0.0368	0.0430	0.0343	0.0256	0.0310
$\dot{m}_h$	lbm/s	0.0040	0.0042	0.0039	0.0039	0.0039
$\dot{m}_{ox}$	lbm/s	0.0312	0.0322	0.0323	0.0325	0.0324
$\dot{m}_o$	lbm/s	1.0050	1.0200	0.9600	0.9040	0.9090
$\dot{m}_f$	lbm/s	0.1726	0.2221	0.1514	0.1330	0.0748
t_b	sec	6.70	6.30	6.05	5.80	5.25
Φ		0.71	0.93	1.41	1.08	0.33
η/η_{ref}		0.88	0.71	0.93	1.00	0.61
$T_{cam\ max}$	°R	1619	1450	1372	1754	1309
$T_{cam\ ave}$	°R	1028	971	818	901	791
$T_{t\ plume}$	°R	X	2150	1800	1260	1280
ε_o		X	0.08	0.04	0.28	0.07
M_b (ε_o=1)	W/m²	28000	32000	22000	62000	17000

B. PLUME SIGNATURE COMPUTER CODES

Attempts were made to compare the measured plume signature results with predictions made using the Standardized Plume Flowfield (SPF) and the Standardized Infrared Radiation Model (SIRRM) codes [Refs. 6,7,& 11].

SPF is a computer code comprised of several subroutines that account for the particle and gas interactions in the nozzle, near surfaces external to the nozzle, the separation area following the exhaust, and the plume area. This code provides for: 1) the modelling of the flow in and the overlap of the nearfields, transition region, and farfields; 2) evaluating the effects of chemical kinetics, two-phase flow and various turbulence models; and 3) the interference of external solid bodies and the subsonic region after the Mach discs. It uses a fully-coupled Navier-Stokes solution for the nearfield and transition regions and constant pressure mixing for the farfield. It features: single and two-phase flow, Mach disc mixing/chemistry, nonuniform composition exhaust, finite-rate and equilibrium chemistry options, and finite-rate chemistry throughout the plume. [Ref. 6:pp. 804,814] Two routines are available for obtaining the plume properties, SCIPPY (shock-capturing inviscid plume model) and SPLITP. Scippy calculates the inviscid flow and shock structure. Splitp accounts for turbulence in the nearfield and farfield. These routines can be run separately or together. [Ref. 7:pp. 191-192]

SIRRM is a six-flux numerical code used to approximate the infrared radiation emitted from isothermal and homogeneous models of missile and aircraft exhaust plumes. It is a code that accounts for atmospheric transmission of the emitted radiation, and couples the absorbing and scattering processes of the particles and molecules in the plumes. It allows for " 1) the important molecular vibration-rotation bands, 2) Mie scattering, 3) nonhomogeneous particulate and gaseous concentrations, and 4) variable temperatures throughout the plume volume " [Ref. 11:p. 426].

Although many man-hours were spent operating the SPF code, the files needed for input to SIRRM were never obtained. The SPF code is very complex and was found to require extensive effort simply to understand the input parameters. Although a new setup routine was made available with the latest revision of the code, the documentation was designed more for experienced SPF operators. In order to help future NPS students in operating this code, an instruction manual was generated and several executable files were compiled to help reduce the confusion.

V. CONCLUSIONS AND RECOMMENDATIONS

A. CONCLUSIONS

The following conclusions were drawn from this investigation:

1. The irradiance/emittance of the plume increased approximately with the second power of the actual combustor stagnation temperature. Increased temperature resulted from equivalence ratios closer to unity, higher energy ingredients and higher obtainable combustion efficiency.

2. The addition of magnesium (Mg) appeared to increase the irradiance/emittance.

3. The addition of silicon (Si) appeared to decrease the irradiance/emittance.

4. A more accurate and faster response time technique is needed for measuring the plume temperature.

5. The metallized M-096 fuel produced approximately the same plume IR signature as HTPB in the 2-5 μm range.

6. At 15 nozzle exit diameters into the plume the approximate Mach number was 0.7, the specific heat ratio was 1.35, and the entrained air to plume gas mixing ratio was approximately 3:1.

7. The effective emissivity of the SFRJ plumes had an average value of approximately 0.2.

B. RECOMMENDATIONS

Testing should continue in this area. Due to the nonavailability of previous test data, the small inventory of some fuels, the long time

required for each test, and the inexperience of the operator, the exact irradiance and performance data were not always obtained.

Future testing should be done with the plume emissivity set at 0.2. Setting the object emissivity initially low will also give a more realistic value of irradiance from the IR camera. It will also reduce the saturation of the plume center when the actual ε_o is used.

Specific interest should be placed on studying the effects of silicon, which appear to decrease the irradiance, and the M-103 composition, which appeared to significantly increase the irradiance.

APPENDIX A

IR DATA RESULTS

A. TEST-3 IR RESULTS:

Fuel:
Type: HTPB
Length: 13.00 inches

IR Camera Data:
Filter: None
Aperture: 2
L_{probe}: 48 inches

Environmental Conditions:
T_{amb}: 524.9 °R
P_{amb}: 14.53 psia

Graph (Right): Temperatures (ε_o=1) from IR camera for 5 sequential frames. Three "spot" functions and one "area" function.
$T_{cam\ ave}$ (ε_o=1): 1248°R

Frame (Below):
Length: 20 inches
Time (into burn): 6.03 sec
$T_{cam\ max}$ (ε_o=1): >1387°R
W_{max}: >20,000 W/m²

Burn Status:
P_{4b}: Unknown
t_b: 7.0 sec
ϕ: Unknown
η: Unknown
$T_{tc\ plume}$: Unknown
ε_o (Calc): Unknown

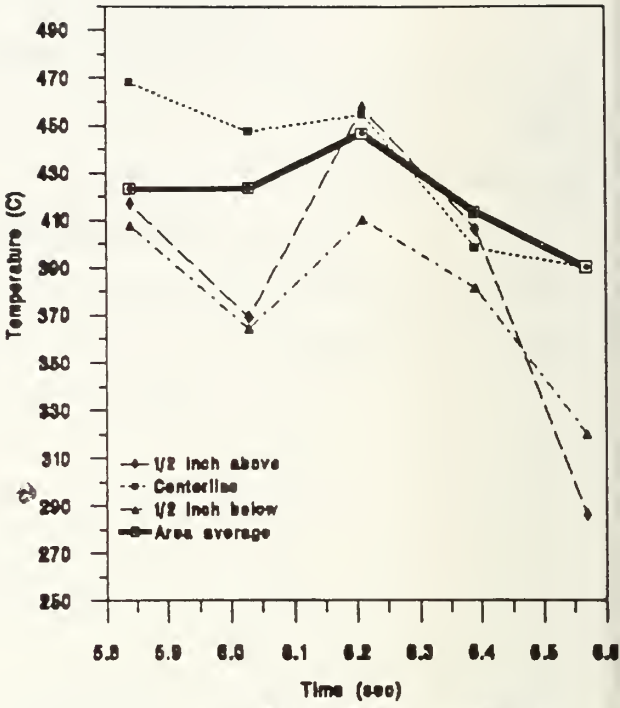

FIGURE A-1: TEST-3: Plume Temperature At 14 Nozzle Diameters From The Nozzle Exit (Based On An Emissivity=1)

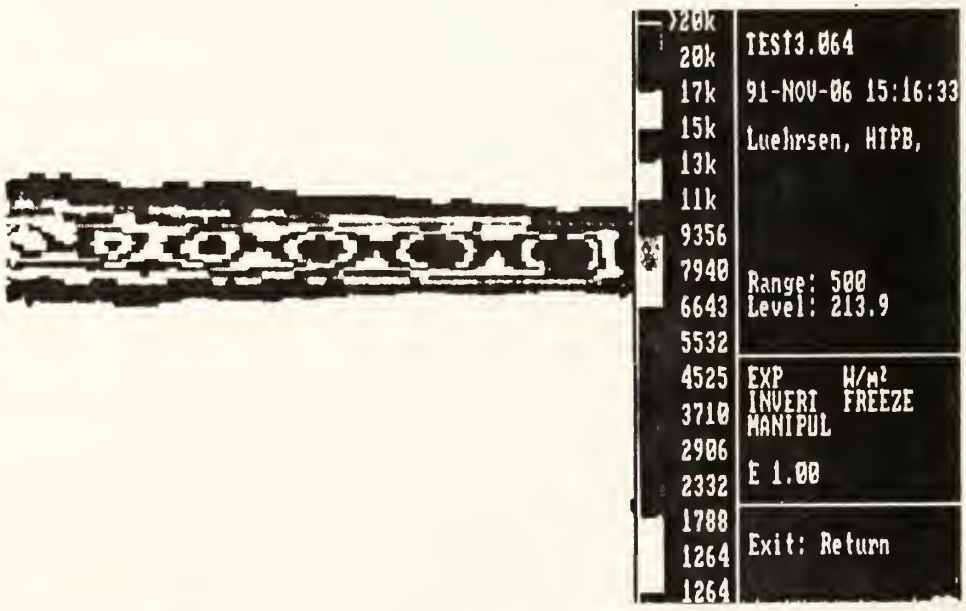

FIGURE A-2: TEST-3: IR Plume Representation

B. TEST-6 IR RESULTS:

Fuel:
Type: PLEXIGLAS
Length: 11.94 inches

IR Camera Data:
Filter: None
Aperture: 2
L_{probe}: 48 inches

Environmental Conditions:
T_{amb}: 524.9 °R
P_{amb}: 14.49 psia

Graph (Right): Temperatures (ε_o=1 from IR camera for 6 sequential frames. Three "spot" functions and one "area" function.
$T_{cam\ ave}$ (ε_o=1): 793°R

Frame (Below):
Length: 20 inches
Time (into burn): 5.29 sec
$T_{cam\ max}$ (ε_o=1): 1226°R
W_{max}: 12,000 W/m²

Burn Status:
P_{4b}: 91
t_b: 7.35 sec
ϕ: 0.79
$T_{tc\ plume}$: 1080°R
ε_o (Calc): 0.20

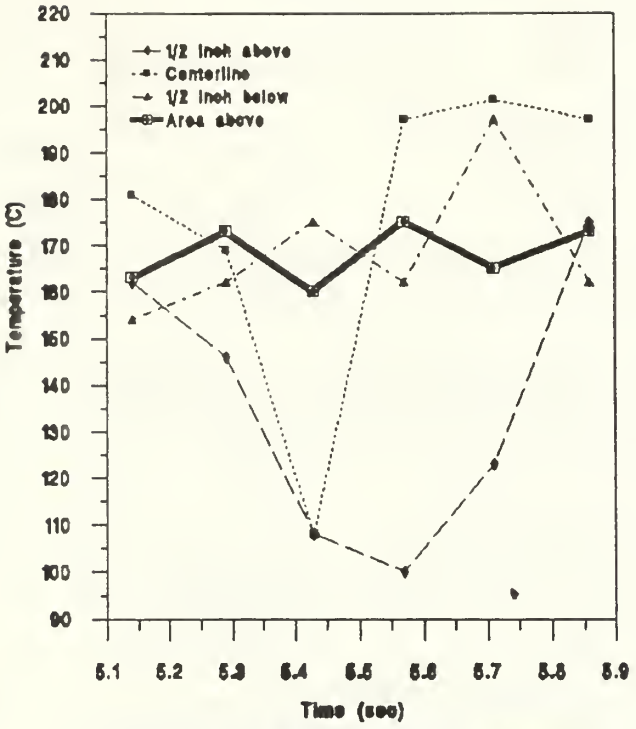

FIGURE A-3: TEST-6: Plume Temperature At 14 Nozzle Diameters From The Nozzle Exit (Based On An Emissivity=1)

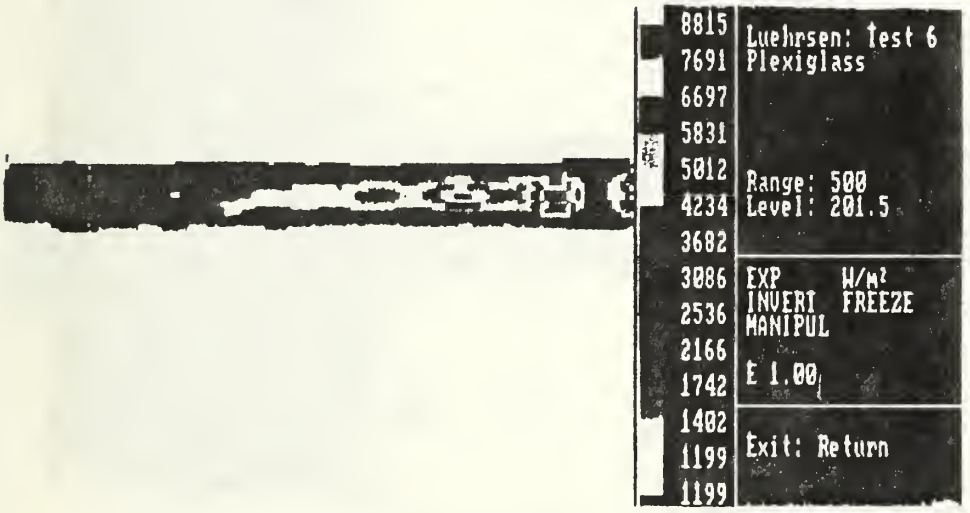

FIGURE A-4: TEST-6: IR Plume Representation

C. TEST-7 IR RESULTS:

Fuel:

Type:	HTPB
Length:	12.06 inches

IR Camera Data:

Filter:	None
Aperture:	2
L_{probe}:	48 inches

Environmental Conditions:

T_{amb}:	524.9 °R
P_{amb}:	14.53 psia

Graph (Right): Temperatures (ε_o=1) from IR camera for 5 sequential frames. Three "spot" functions and one "area" function.

$T_{cam\ ave}$ (ε_o=1): 1183°R

Frame (Below):

Length:	20 inches
Time (into burn):	4.23 sec
$T_{cam\ max}$ (ε_o=1):	>1412°R
W_{max}:	>21000 W/m²

Burn Status:

P_{4b}:	107
t_b:	6.70 sec
ϕ:	1.18
$T_{tc\ plume}$:	1480°R
ε_o (Calc):	0.50

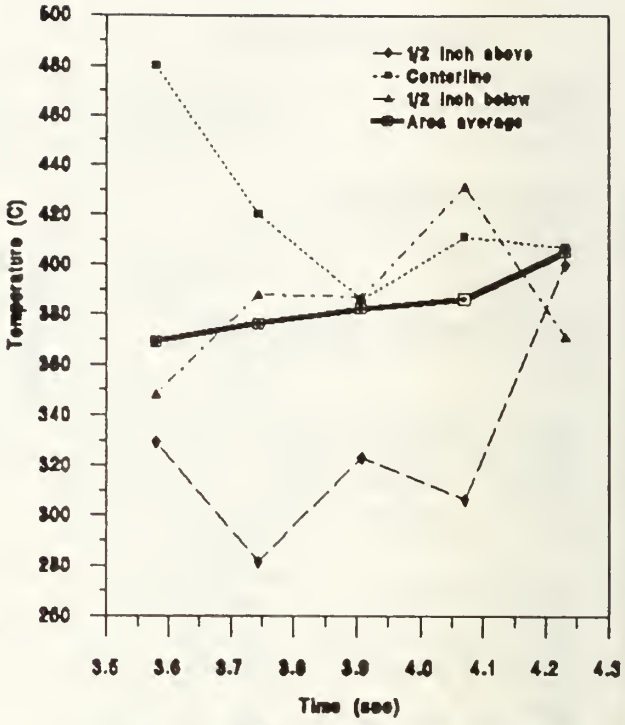

FIGURE A-5: TEST-7: Plume Temperature At 14 Nozzle Diameters From The Nozzle Exit (Based On An Emissivity=1)

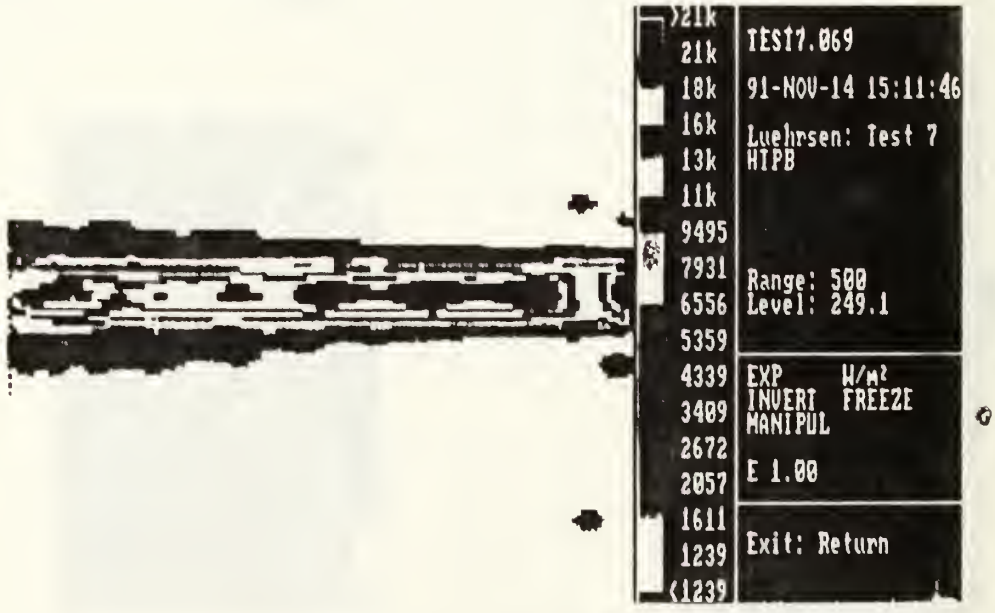

FIGURE A-6: TEST-7: IR Plume Representation

D. TEST-9 IR RESULTS:

Fuel:
Type: HTPB
Length: 13.00 inches

IR Camera Data:
Filter: None
Aperture: 2
L_{probe}: 48 inches

Environmental Conditions:
T_{amb}: 521.7 °R
P_{amb}: 14.53 psia

Graph (Right): Temperatures (ε_o=1) from IR camera for 5 sequential frames. Three "spot" functions and one "area" function.
$T_{cam\ ave}$ (ε_o=1): 1187°R

Frame (Below):
Length: 20 inches
Time (into burn): 5.88 sec
$T_{cam\ max}$ (ε_o=1): >1412°R
W_{max}: >21000 W/m²

Burn Status:
P_{4b}: 122
t_b: 9.30 sec
ϕ: 1.07
$T_{tc\ plume}$: Unknown
ε_o (Calc): Unknown

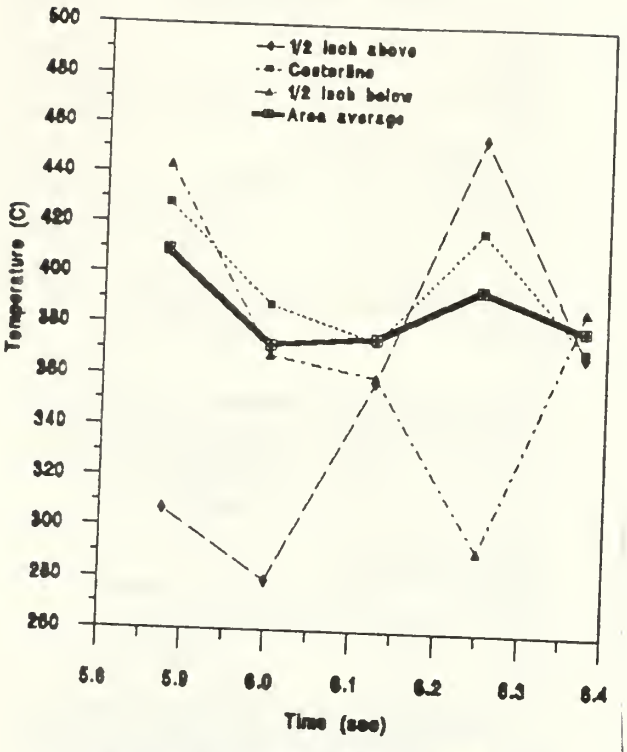

FIGURE A-7: TEST-9: Plume Temperature At 14 Nozzle Diameters From The Nozzle Exit (Based On An Emissivity=1)

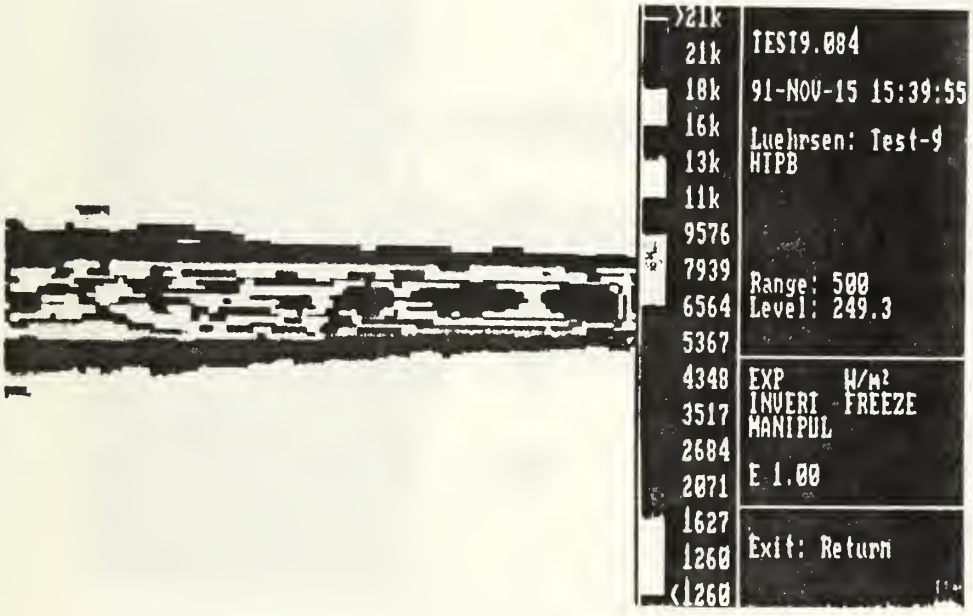

FIGURE A-8: TEST-9: IR Plume Representation

E. TEST-12 IR RESULTS:

Fuel:
Type: HTPB
Length: 6.438 inches

IR Camera Data:
Filter: None
Aperture: 0
L_{probe}: 60 inches

Environmental Conditions:
T_{amb}: 515.9 °R
P_{amb}: 14.71 psia

Graph (Right): Temperatures (ε_o=1) from IR camera for 5 sequential frames. Three "spot" functions and one "area" function.
$T_{cam\ ave}$ (ε_o=1): 685°R

Frame (Below):
Length: 26 inches
Time (into burn): 6.74 sec
$T_{cam\ max}$ (ε_o=1): >805°R
W_{max}: >2271 W/m²

Burn Status:
P_{4b}: 88.5 psia
t_b: 8.00 sec
ϕ: 0.44
$T_{tc\ plume}$: 895°R
$T_{t\ plume}$: 1070°R
ε_o (Calc): 0.17

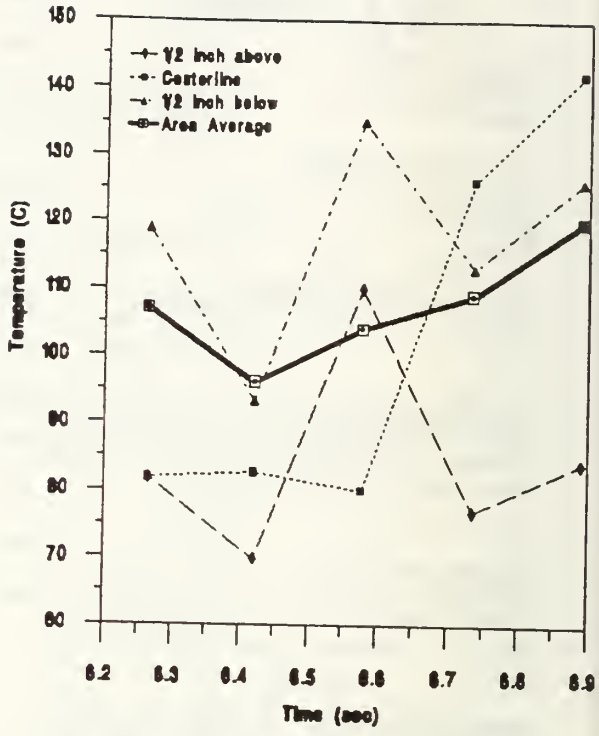

FIGURE A-9: TEST-12: Plume Temperature At 18.7 Nozzle Diameters From The Nozzle Exit (Based On An Emissivity=1)

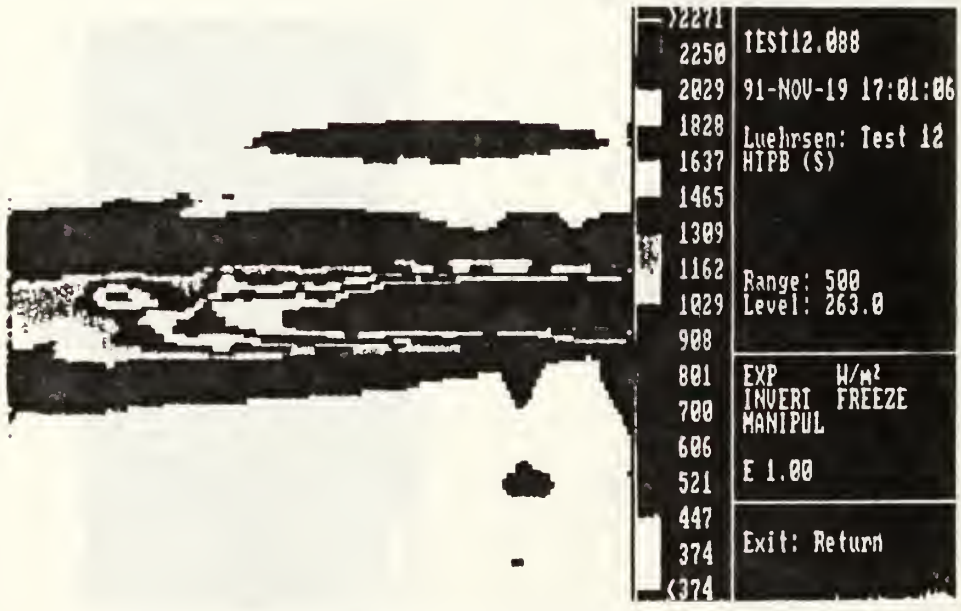

FIGURE A-10: TEST-12: IR Plume Representation

F. TEST-14 IR RESULTS:

Fuel:
Type: M-096 (No Mg)
Length: 6.50 inches

IR Camera Data:
Filter: None
Aperture: 1
L_{probe}: 60 inches

Environmental Conditions:
T_{amb}: 521.0 °R
P_{amb}: 14.73 psia

Graph (Right): Temperatures (ε_o=1) from IR camera for 5 sequential frames. Three "spot" functions and one "area" function.
$T_{cam\ ave}$ (ε_o=1): 821°R

Frame (Below):
Length: 26 inches
Time (into burn): 6.41 sec
$T_{cam\ max}$ (ε_o=1): >1075°R
W_{max}: >7224 W/m²

Burn Status:
P_{4b}: 87 psia
t_b: 7.50 sec
ϕ: 0.54
$T_{tc\ plume}$: 900°R
$T_{t\ plume}$: 1200°R
ε_o (Calc): 0.22

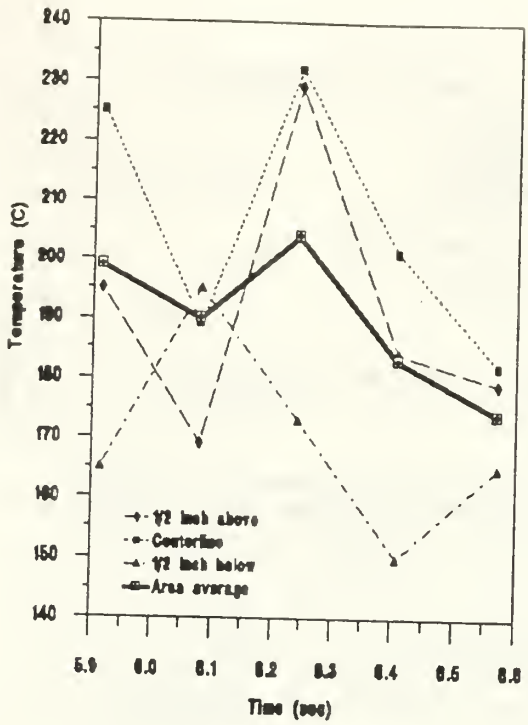

FIGURE A-11: TEST-14: Plume Temperature At 18.7 Nozzle Diameters From The Nozzle Exit (Based On An Emissivity=1)

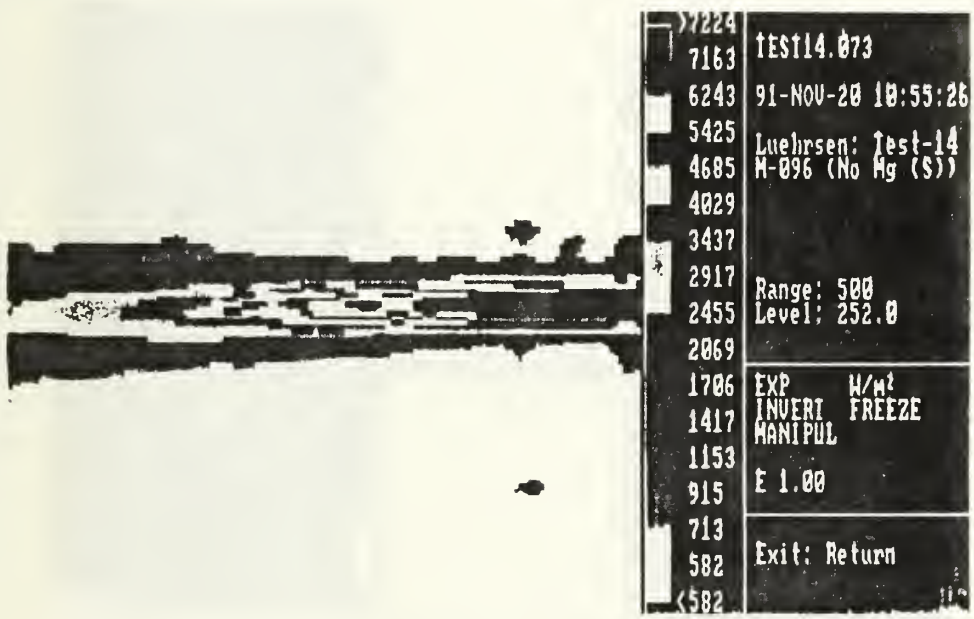

FIGURE A-12: TEST-14: IR Plume Representation

G. TEST-15 IR RESULTS:

Fuel:
Type: M-104
Length: 6.44 inches

IR Camera Data:
Filter: None
Aperture: 1
L_{probe}: 60 inches

Environmental Conditions:
T_{amb}: 521.0 °R
P_{amb}: 14.71 psia

Graph: The temperatures (ε_o=1) were all less than the minimum for the IR camera.
$T_{cam\ ave}$ (ε_o=1): <852°R

Frame (Below):
Length: 26 inches
Time (into burn): 4.00 sec
$T_{cam\ max}$ (ε_o=1): >1130°R
W_{max}: >8759 W/m²

Burn Status:
P_{4b}: Unknown
t_b: Unknown
ϕ: Unknown
$T_{tc\ plume}$: Unknown
$T_{t\ plume}$: Unknown
ε_o (Calc): Unknown

NO GRAPH AVIABLE DUE TO ALL TEMPERATURE BEING LESS THE MINIMUM FOR THE IR CAMERA SETTINGS.

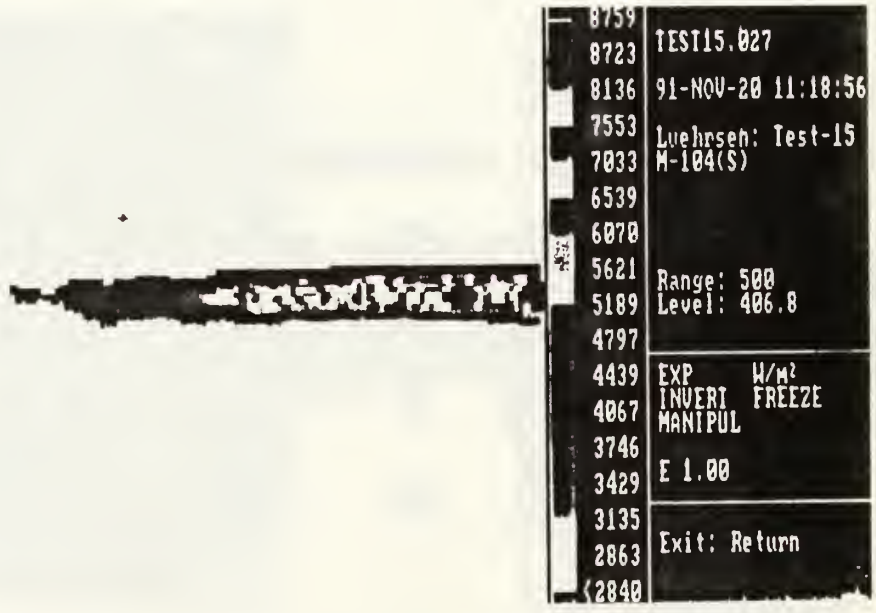

FIGURE A-13: TEST-15: IR Plume Representation

H. TEST-16 IR RESULTS:

Fuel:
Type: M-104
Length: 6.47 inches

IR Camera Data:
Filter: None
Aperture: 1
L_{probe}: 60 inches

Environmental Conditions:
T_{amb}: 521.0 °R
P_{amb}: 14.56 psia

Graph (Right): Temperatures (ε_o=1) from IR camera for 4 sequential frames. Three "spot" functions and one "area" function.
$T_{cam\ ave}$ (ε_o=1): 825°R

Frame (Below):
Length: 26 inches
Time (into burn): 5.00 sec
$T_{cam\ max}$ (ε_o=1): >1129°R
W_{max}: >8761 W/m²

Burn Status:
P_{4b}: 102 psia
t_b: 6.35 sec
ϕ: 0.30
$T_{tc\ plume}$: 1005°R
$T_{t\ plume}$: 1430°R
ε_o (Calc): 0.14

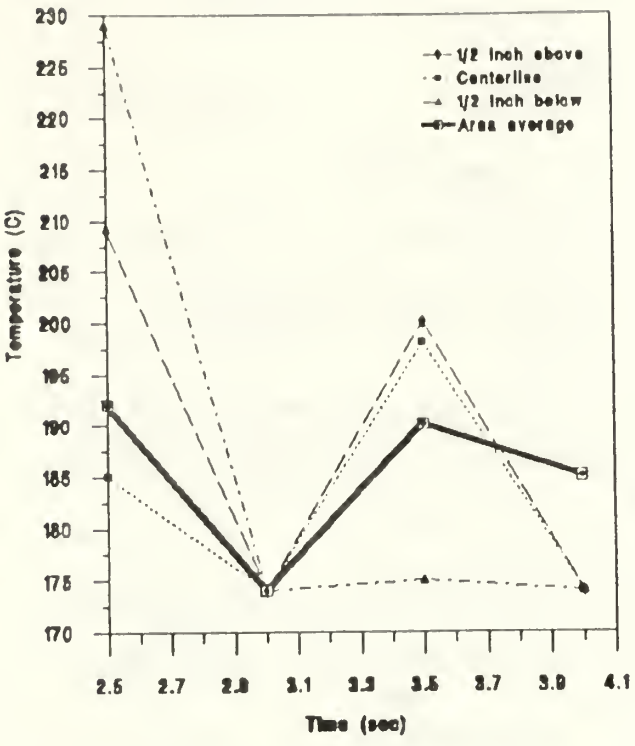

FIGURE A-14: TEST-16: Plume Temperature At 16.7 Nozzle Diameters From The Nozzle Exit (Based On An Emissivity=1)

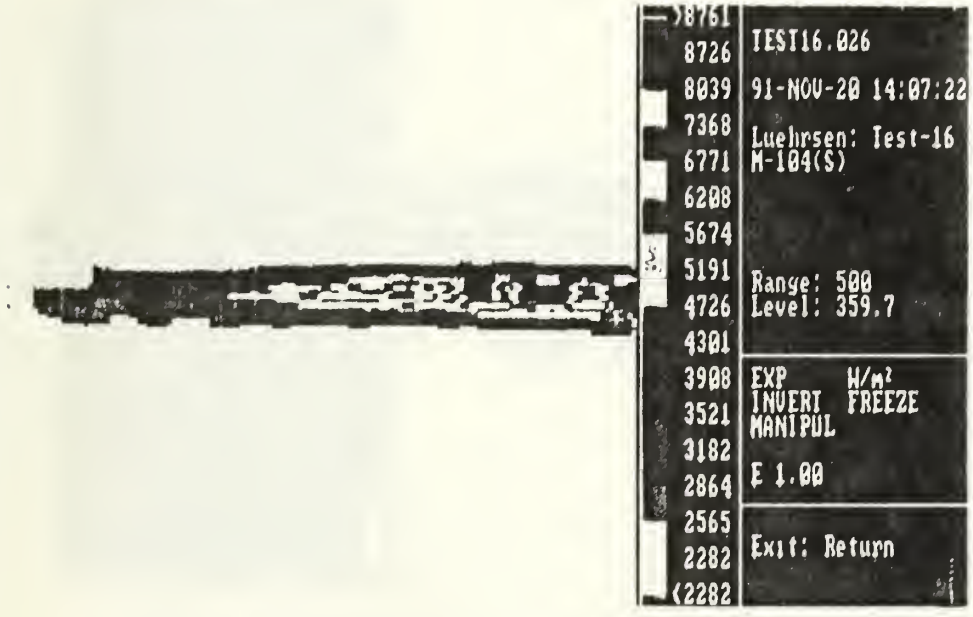

FIGURE A-15: TEST-16: IR Plume Representation

I. TEST-17 IR RESULTS:

Fuel:

Type:	M-105
Length:	6.50 inches

IR Camera Data:

Filter:	None
Aperture:	1
L_{probe}:	60 inches

Environmental Conditions:

T_{amb}:	524.9 °R
P_{amb}:	14.71 psia

Graph (Right): Temperatures (ε_o=1) from IR camera for 6 sequential frames. Three "spot" functions and one "area" function.

$T_{cam\ ave}$ (ε_o=1): 1012°R

Frame (Below):

Length:	26 inches
Time (into burn):	6.67 sec
$T_{cam\ max}$ (ε_o=1):	>>1091°R
W_{max}:	>>7651 W/m²

Burn Status:

P_{4b}:	105 psia
t_b:	6.20 sec
ϕ:	0.33
$T_{tc\ plume}$:	1250°R
$T_{t\ plume}$:	1550°R
ε_o (Calc):	0.39

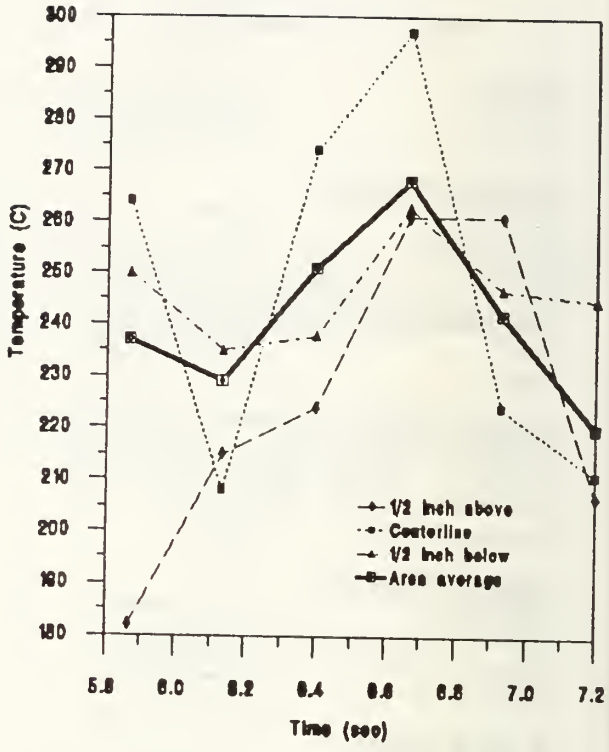

FIGURE A-16: TEST-17: Plume Temperature At 16.7 Nozzle Diameters From The Nozzle Exit (Based On An Emissivity=1)

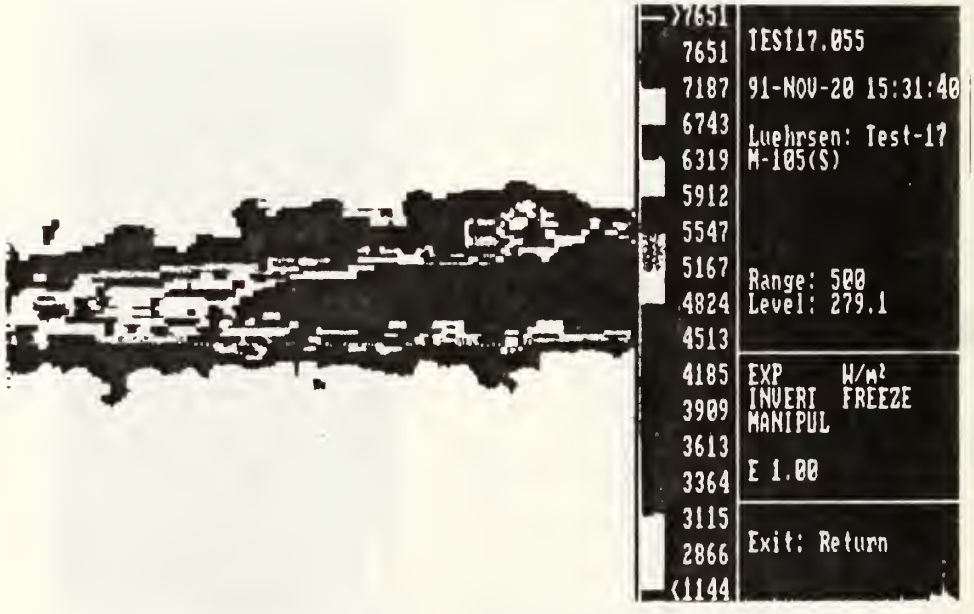

FIGURE A-17: TEST-17: IR Plume Representation

J. TEST-18 IR RESULTS:

Fuel:
Type: M-096 (No Mg)
Length: 13.06 inches

IR Camera Data:
Filter: None
Aperture: 2
L_{probe}: 60 inches

Environmental Conditions:
T_{amb}: 524.9 °R
P_{amb}: 14.65 psia

Graph (Right): Temperatures (ε_o=1) from IR camera for 5 sequential frames. Three "spot" functions and one "area" function.
$T_{cam\ ave}$ (ε_o=1): 1223°R

Frame (Below):
Length: 26 inches
Time (into burn): 2.57 sec
$T_{cam\ max}$ (ε_o=1): >1444°R
W_{max}: >23000 W/m²

Burn Status:
P_{4b}: 120 psia
t_b: 6.35 sec
ϕ: 1.1150
$T_{tc\ plume}$: 1600°R
$T_{t\ plume}$: 2000°R
ε_o (Calc): 0.20

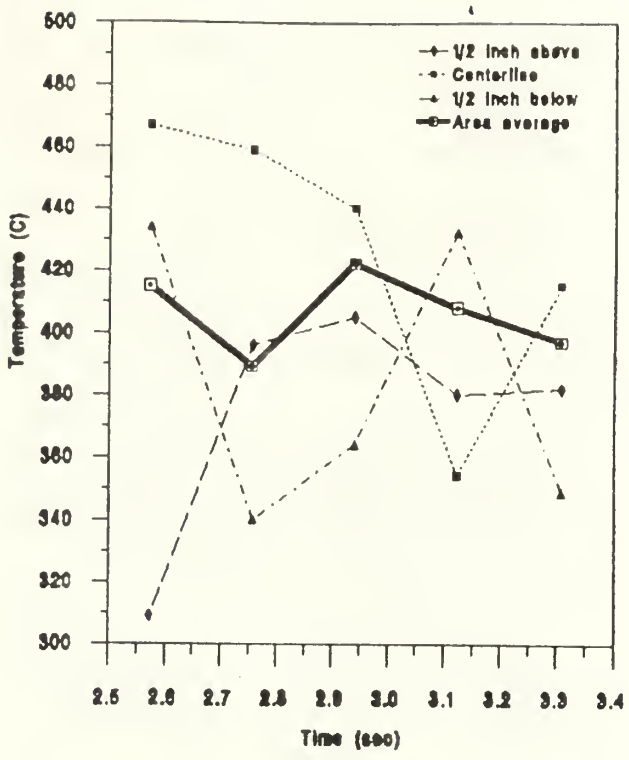

FIGURE A-18: TEST-18: Plume Temperature At 16.7 Nozzle Diameters From The Nozzle Exit (Based On An Emissivity=1)

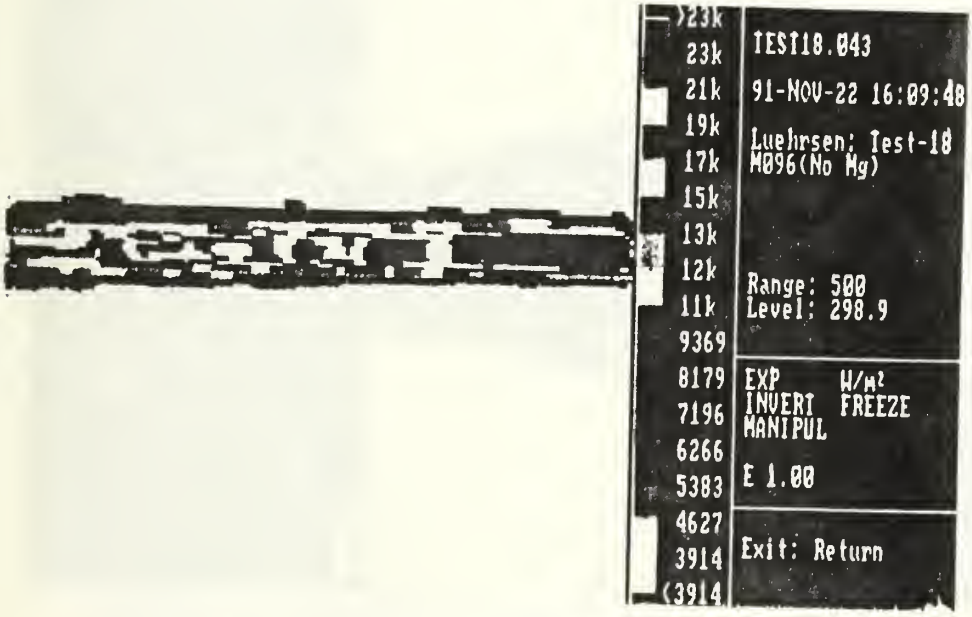

FIGURE A-19: TEST-18: IR Plume Representation

K. TEST-19 IR RESULTS:

Fuel:

Type:	M-096
Length:	13.00 inches

IR Camera Data:

Filter:	None
Aperture:	2
L_{probe}:	60 inches

Environmental Conditions:

T_{amb}:	521.7 °R
P_{amb}:	14.69 psia

Graph (Right): Temperatures (ε_o=1) from IR camera for 5 sequential frames. Three "spot" functions and one "area" function.

$T_{cam\ ave}$ (ε_o=1): 1217°R

Frame (Below):

Length:	26 inches
Time (into burn):	5.54 sec
$T_{cam\ max}$ (ε_o=1):	>>1412°R
W_{max}:	>>21000 W/m²

Burn Status:

P_{4b}:	107 psia
t_b:	5.55 sec
ϕ:	1.31
$T_{tc\ plume}$:	1800°R
$T_{t\ plume}$:	2160°R
ε_o (Calc):	0.16

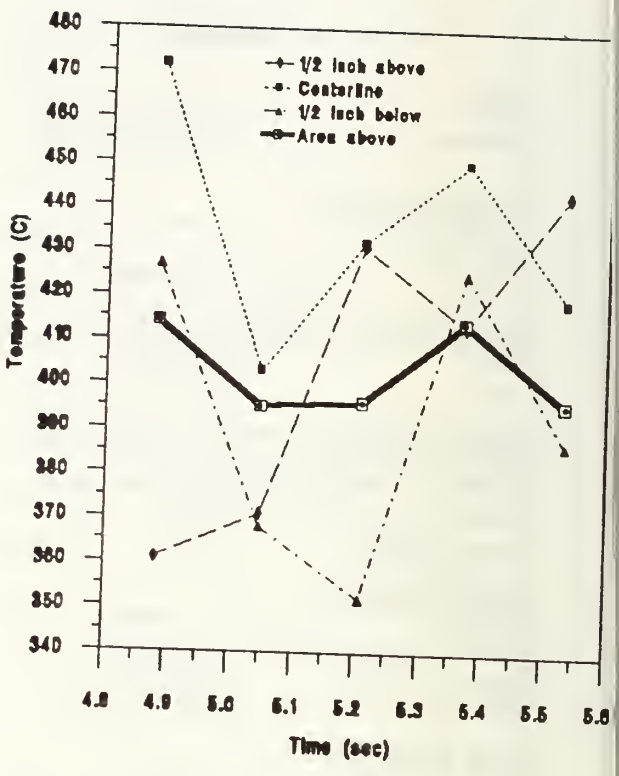

FIGURE A-20: TEST-19: Plume Temperature At 16.7 Nozzle Diameters From The Nozzle Exit (Based On An Emissivity=1)

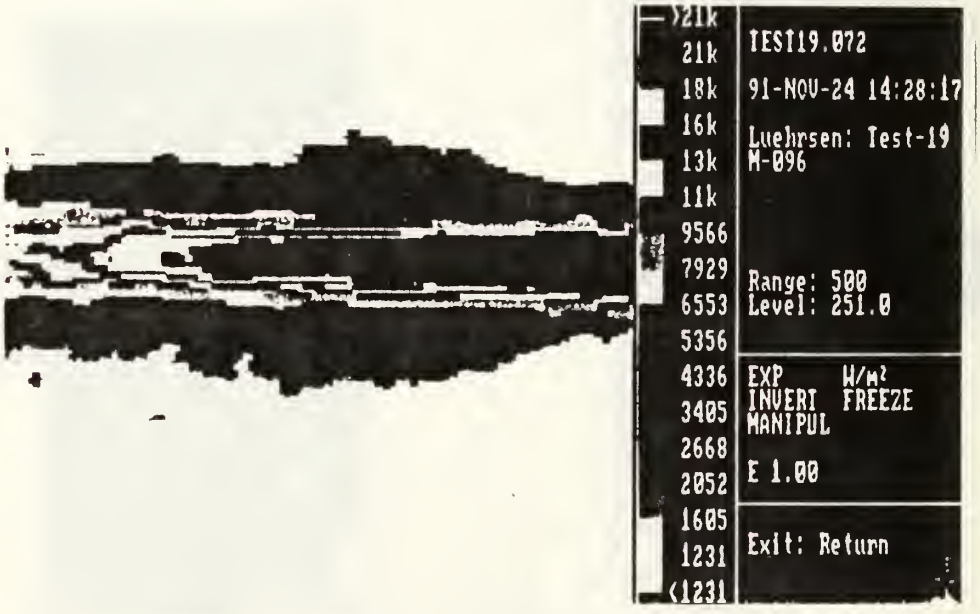

FIGURE A-21: TEST-19: IR Plume Representation

L. TEST-20 IR RESULTS:

Fuel:

Type:	M-104
Length:	12.94 inches

IR Camera Data:

Filter:	Glass
Aperture:	1
L_{probe}:	60 inches

Environmental Conditions:

T_{amb}:	530.0 °R
P_{amb}:	16.14 psia

Graph (Right): Temperatures (ε_o=1) from IR camera for 5 sequential frames. Three "spot" functions and one "area" function.

$T_{cam\ ave}$ (ε_o=1):	1028°R

Frame (Below):

Length:	26 inches
Time (into burn):	4.73 sec
$T_{cam\ max}$ (ε_o=1):	1619°R
W_{max}:	28000 W/m²

Burn Status:

P_{4b}:	173 psia
t_b:	6.70 sec
ϕ:	0.70
$T_{tc\ plume}$:	Unknown
$T_{t\ plume}$:	Unknown
ε_o (Calc):	Unknown

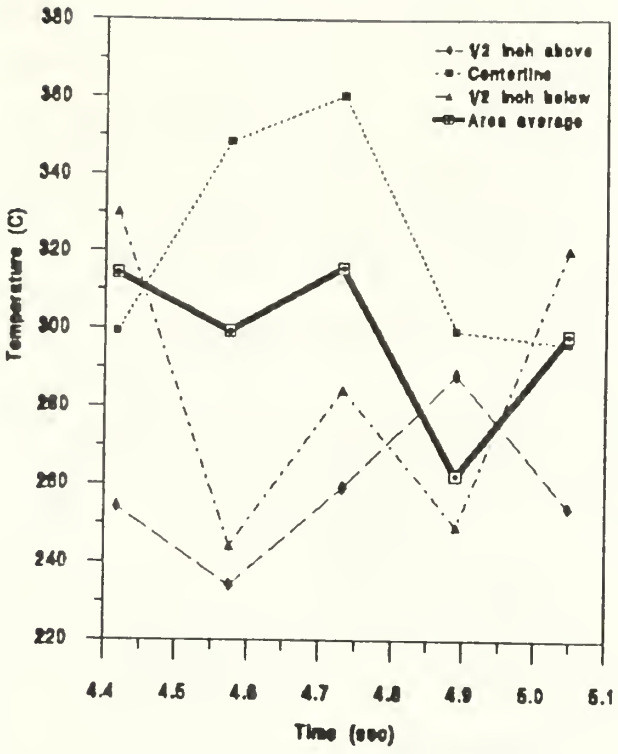

FIGURE A-22: TEST-20: Plume Temperature At 16.7 Nozzle Diameters From The Nozzle Exit (Based On An Emissivity=1)

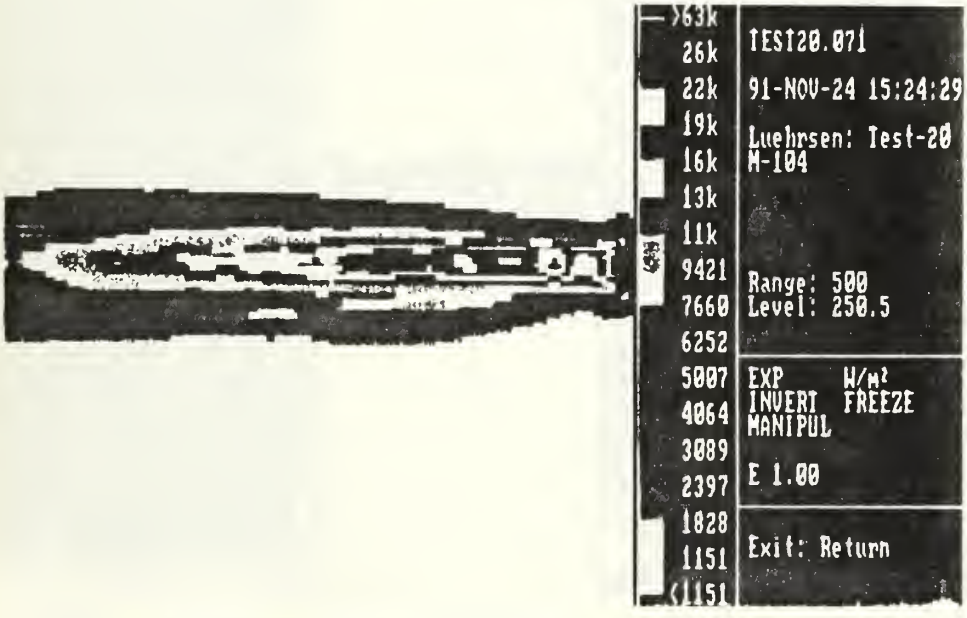

FIGURE A-23: TEST-20: IR Plume Representation

M. TEST-21 IR RESULTS:

Fuel:

Type:	M-105
Length:	13.00 inches

IR Camera Data:

Filter:	Glass
Aperture:	1
L_{probe}:	60 inches

Environmental Conditions:

T_{amb}:	524.6 °R
P_{amb}:	16.12 psia

Graph (Right): Temperatures (ε_o=1) from IR camera for 5 sequential frames. Three "spot" functions and one "area" function.

$T_{cam\ ave}$ (ε_o=1): 971°R

Frame (Below):

Length:	26 inches
Time (into burn):	5.21 sec
$T_{cam\ max}$ (ε_o=1):	1450°R
W_{max}:	32000 W/m²

Burn Status:

P_{4b}:	147 psia
t_b:	6.30 sec
ϕ:	0.88
$T_{tc\ plume}$:	2100°R
$T_{t\ plume}$:	2150°R
ε_o (Calc):	0.08

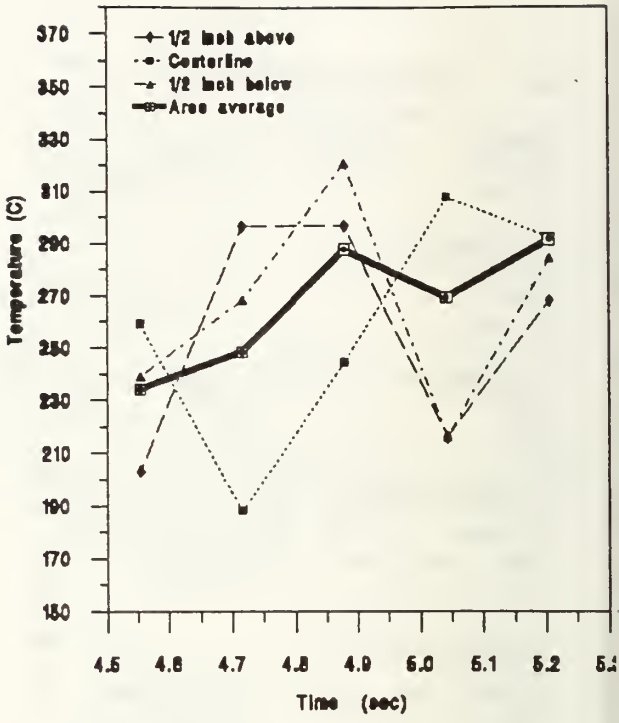

FIGURE A-24: TEST-21: Plume Temperature At 16.7 Nozzle Diameters From The Nozzle Exit (Based On An Emissivity=1)

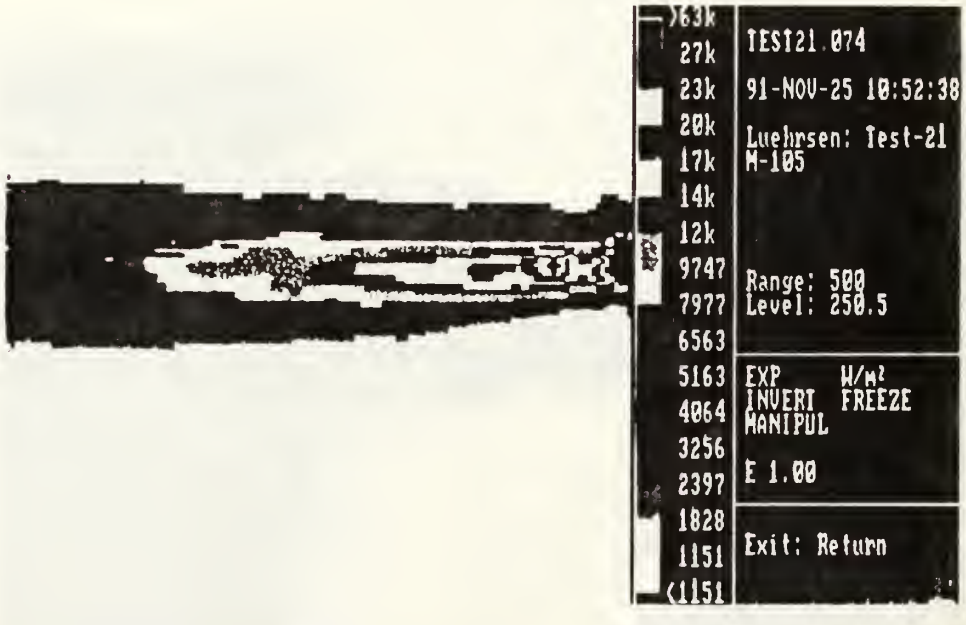

FIGURE A-25: TEST-21: IR Plume Representation

N. TEST-22 IR RESULTS:

Fuel:
Type: M-106
Length: 13.07 inches

IR Camera Data:
Filter: Glass
Aperture: 1
L_{probe}: 60 inches

Environmental Conditions:
T_{amb}: 524.6 °R
P_{amb}: 16.11 psia

Graph (Right): Temperatures (ε_o=1) from IR camera for 5 sequential frames. Three "spot" functions and one "area" function.
$T_{cam\ ave}$ (ε_o=1): 818°R

Frame (Below):
Length: 26 inches
Time (into burn): 4.28 sec
$T_{cam\ max}$ (ε_o=1): 1372°R
W_{max}: 22000 W/m²

Burn Status:
P_{4b}: 137 psia
t_b: 6.05 sec
ϕ: 1.41
$T_{tc\ plume}$: 1300°R
$T_{t\ plume}$: 1800°R
ε_o (Calc): 0.04

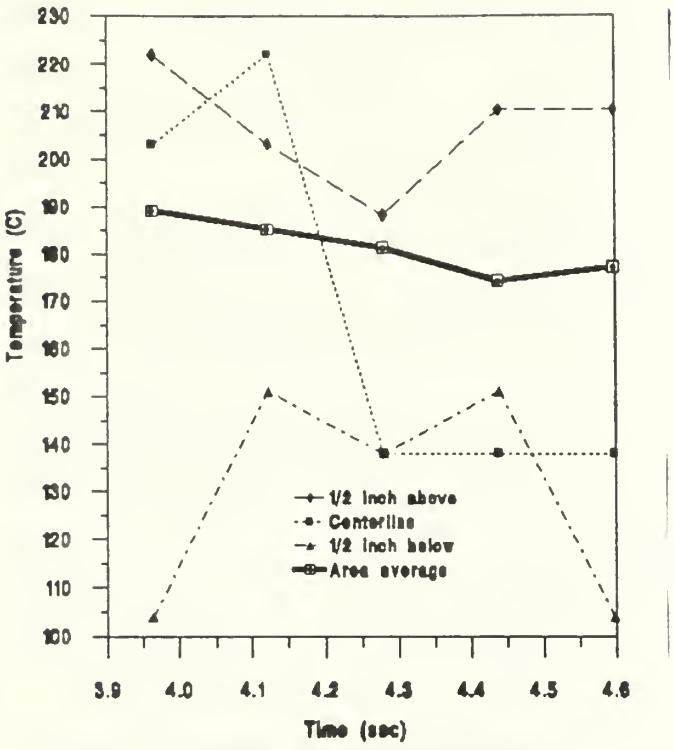

FIGURE A-26: TEST-22: Plume Temperature At 16.7 Nozzle Diameters From The Nozzle Exit (Based On An Emissivity=1)

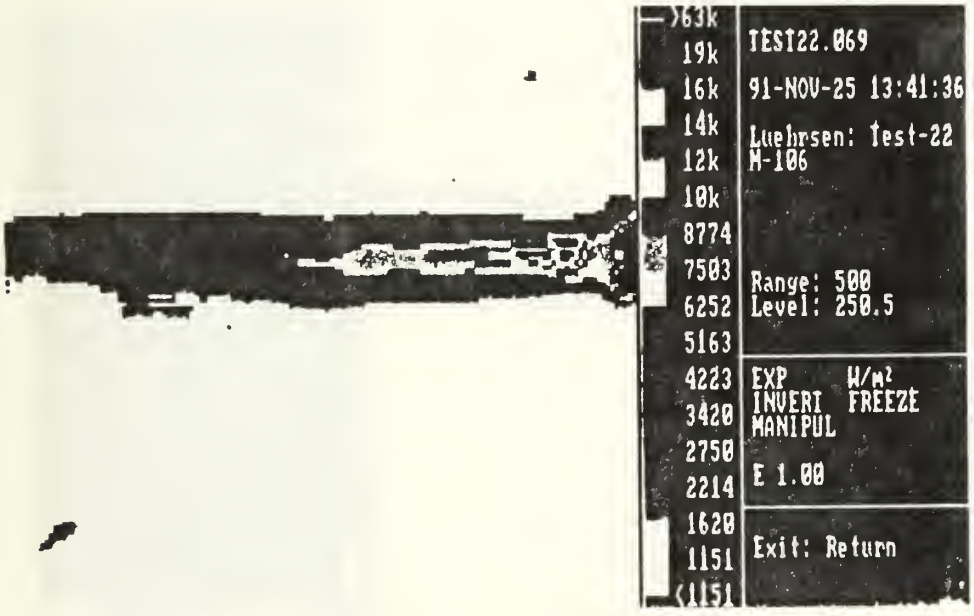

FIGURE A-27: TEST-22: IR Plume Representation

O. TEST-23 IR RESULTS:

Fuel:

Type:	M-103
Length:	12.88 inches

IR Camera Data:

Filter:	Glass
Aperture:	1
L_{probe}:	60 inches

Environmental Conditions:

T_{amb}:	524.6 °R
P_{amb}:	14.66 psia

Graph (Right): Temperatures (ε_o=1) from IR camera for 5 sequential frames. Three "spot" functions and one "area" function.

$T_{cam\ ave}$ (ε_o=1):	901°R

Frame (Below):

Length:	26 inches
Time (into burn):	3.58 sec
$T_{cam\ max}$ (ε_o=1):	1754°R
W_{max}:	62000 W/m²

Burn Status:

P_{tb}:	125 psia
t_b:	5.80 sec
ϕ:	1.08
$T_{tc\ plume}$:	1080°R
$T_{t\ plume}$:	1260°R
ε_o (Calc):	0.28

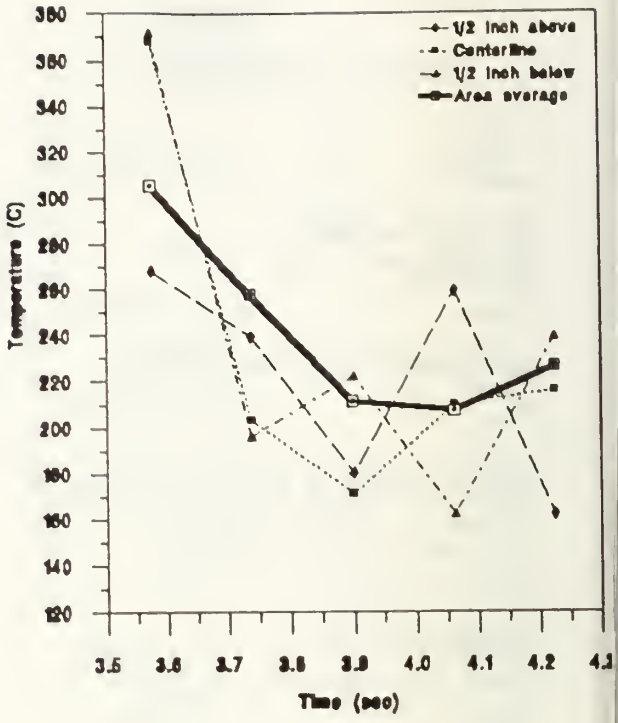

FIGURE A-28: TEST-23: Plume Temperature At 18.7 Nozzle Diameters From The Nozzle Exit (Based On An Emissivity=1)

FIGURE A-29: TEST-23: IR Plume Representation

P. TEST-24 IR RESULTS:

Fuel:
Type: M-105
Length: 6.47 inches

IR Camera Data:
Filter: None
Aperture: 2
L_{probe}: 60 inches

Environmental Conditions:
T_{amb}: 523.1 °R
P_{amb}: 14.65 psia

Graph (Right): Temperatures (ε_o=1) from IR camera for 5 sequential frames. Three "spot" functions and one "area" function.
$T_{cam\ ave}$ (ε_o=1): 791°R

Frame (Below):
Length: 26 inches
Time (into burn): 5.02 sec
$T_{cam\ max}$ (ε_o=1): 1309°R
W_{max}: 17000 W/m²

Burn Status:
P_{tb}: 91 psia
t_b: 5.25 sec
ϕ: 0.33
$T_{tc\ plume}$: 870°R
$T_{t\ plume}$: 1280°R
ε_o (Calc): 0.07

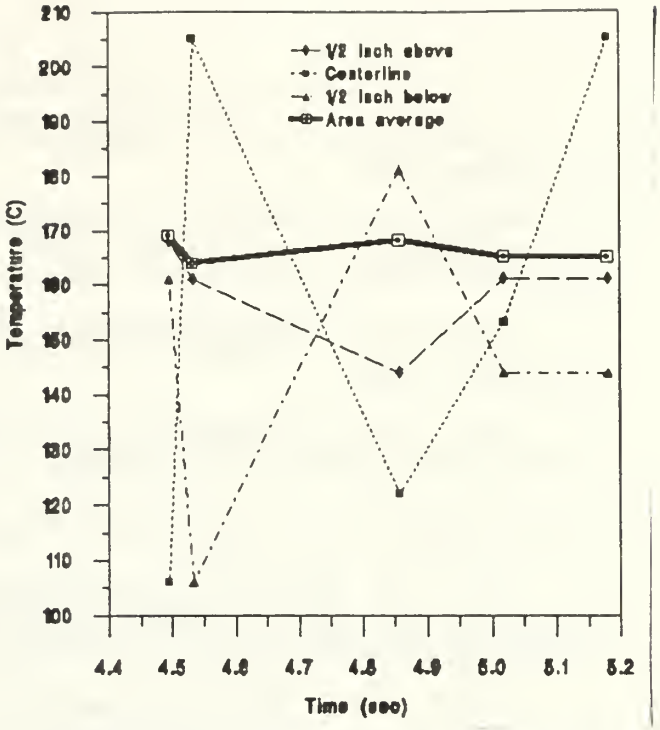

FIGURE A-30: TEST-24: Plume Temperature At 16.7 Nozzle Diameters From The Nozzle Exit (Based On An Emissivity=1)

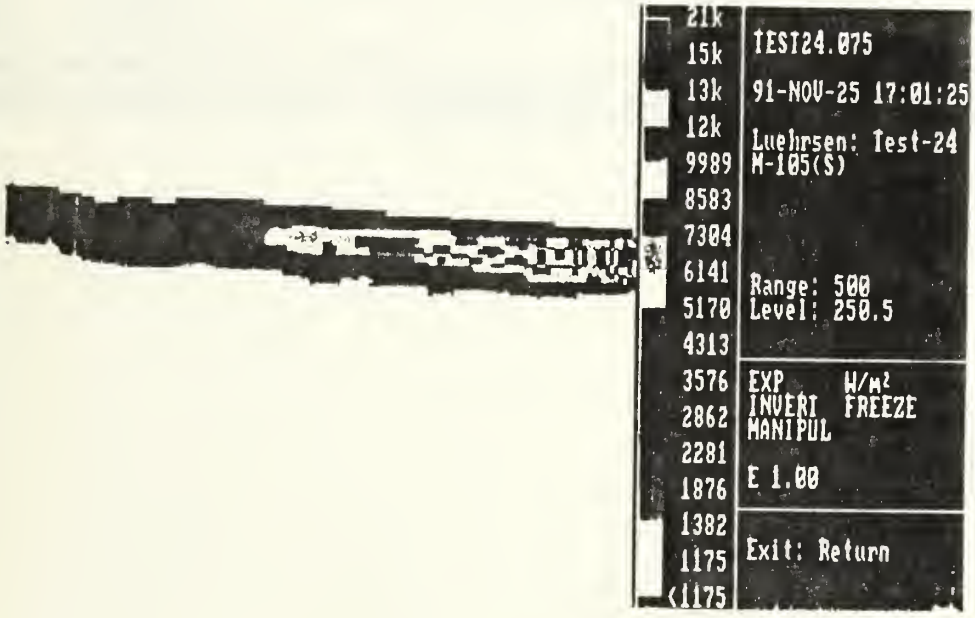

FIGURE A-31: TEST-24: IR Plume Representation

LIST OF REFERENCES

1. Netzer, D.W., AE-4452 Classroom Notes, Naval Postgraduate School, March-June 1991.

2. Netzer, D.W. and Gany, A.,Fuel Performance Evaluation for the Solid-Fueled Ramjet, International Journal of Turbo and Jet Engines 2, Martinus Nijhoff Publishers, London, 1985.

3. Billig, F.S., Tactical Missile Design Concepts, Johns Hopkins University, Applied Physics Laboratory Technical Digest, Vol. 4, No. 3, July-Sept 1983.

4. Ball, R.E., The Fundamentals of Aircraft Combat Survivability Analysis and Design; AIAA, Publication Series, Washington, D.C., 1985.

5. Spiro, I.J. and Schlessinger, M., Infrared Technology Fundamentals, Marcel Dekker, Inc., New York, NY, 1989.

6. Dash, S.M. Analysis of Exhaust Plumes and Their Interaction with Missile Airframes in Tactical Missiles Aerodynamics, Vol 104, American Institute of Aeronautics and Astronautics, Inc (AIAA), 1986.

7. Victor, A.C., Plume Considerations, to be published by AIAA, 1992.

8. MDAS/DCALC User's Guide, Document M4490, First Ed., Rev. 0., Kaye Instruments, Beford, Ma., 1990.

9. Thermovision 870 Operating Manual, AMEGA Infrared Systems AB, 1986.

10. Cruise, D.R., "Theoretical Computations of Equilibrium Composition, Thermodynamic Properties, and Performance Characteristics of Propellant Systems", Naval Weapons Center Report NWC TP 6037, Revision 1, Nov. 1991.

11. Dash, S.M., Pearce, B.E., Pergament, H.S., and Fishburne, E.S., Prediction of Rocket Plume Flowfields for Infrared Signature Studies, Vol 17, No 3, May-June 1980, AIAA, 1980.

INITIAL DISTRIBUTION LIST

		No. Copies
1.	Defence Technical Information Center Cameron Station Arlington, Virginia 22304-6145	2
2.	Library, Code 52 Naval Postgraduate School Monterey, California 93943-5002	2
3.	Department Chairman, Code AA Department of Aeronautics and Astronautics Naval Postgraduate School Monterey, California 93943-5000	2
4.	Professor D.W. Netzer, Code AA/Nt Department of Aeronautics and Astronautics Naval Postgraduate School Monterey, California 93943-5000	2
5.	Professor R.P. Shreeve, Code AA/Sf Department of Aeronautics and Astronautics Naval Postgraduate School Monterey, California 93943-5000	2
6.	Mr. F. Zarlingo, Code 3246 Naval Weapons Center China Lake, California 93555	1
7.	R.P. Luehrsen 5601 Selford Rd Baltimore, Maryland 21227	2